Acta Crystallographica Section D
Biological Crystallography
ISSN 0907-4449

X-ray-induced deterioration of disulfide bridges at atomic resolution

Tatiana Petrova,[a,b] Stephan Ginell,[a] Andre Mitschler,[c] Youngchang Kim,[a] Vladimir Y. Lunin,[b] Grazyna Joachimiak,[a] Alexandra Cousido-Siah,[c] Isabelle Hazemann,[c] Alberto Podjarny,[c] Krzysztof Lazarski[a] and Andrzej Joachimiak[a]*

[a]Structural Biology Center, Biosciences Division, Argonne National Laboratory, Argonne, Illinois 60439, USA, [b]Institute of Mathematical Problems of Biology, Russian Academy of Sciences, Pushchino 142290, Russia, and [c]Département de Biologie Structurale et Génomique, IGBMC, CNRS, ULP, INSERM, 1 Rue Laurent Fries, BP 163, 67404 Illkirch, France

Correspondence e-mail: andrzejj@anl.gov

Received 8 April 2010
Accepted 23 August 2010

PDB References: porcine pancreatic elastase, model M1, 100 K, 3mnb; model M2, 100 K, 3mnc; model M3, 100 K, 3mns; model M4, 100 K, 3mnx; model M5, 100 K, 3mo3; model M6, 100 K, 3mo6; model M7, 100 K, 3mo9; model M8, 100 K, 3moc; model A1, 100 K, 3mty; model A2, 100 K, 3odf; model A3, 100 K, 3mu0; model A5, 100 K, 3mu1; model B1, 15 K, 3mu4; model B2, 15 K, 3odd; model B3, 15 K, 3mu5; model B5, 15 K, 3mu8.

Overall and site-specific X-ray-induced damage to porcine pancreatic elastase was studied at atomic resolution at temperatures of 100 and 15 K. The experiments confirmed that irradiation causes small movements of protein domains and bound water molecules in protein crystals. These structural changes occur not only at 100 K but also at temperatures as low as 15 K. An investigation of the deterioration of disulfide bridges demonstrated the following. (i) A decrease in the occupancy of S^{γ} atoms and the appearance of new cysteine rotamers occur simultaneously. (ii) The occupancy decrease is observed for all S^{γ} atoms, while new rotamers arise for some of the cysteine residues; the appearance of new conformations correlates with the accessibility to solvent. (iii) The sum of the occupancies of the initial and new conformations of a cysteine residue is approximately equal to the occupancy of the second cysteine residue in the bridge. (iv) The most pronounced changes occur at doses below 1.4×10^7 Gy, with only small changes occurring at higher doses. Comparison of the radiation-induced changes in an elastase crystal at 100 and 15 K suggested that the dose needed to induce a similar level of deterioration of the disulfide bonds and atomic displacements at 15 K to those seen at 100 K is more than two times higher.

1. Introduction

The hard X-rays used for structure determination can damage protein molecules and in some cases, for example when collecting data from very small crystals or from crystals of very large assemblies, this can be a serious impediment. Therefore, a detailed understanding of radiation damage in protein crystals is of great interest not only for practical crystallography but also for biological interpretation of structural data at the atomic level. Such knowledge may also provide hints on how to mitigate X-ray damage.

Radiation damage manifests itself at two levels: (i) as specific chemical and structural changes in the protein molecule and (ii) as global effects related to general crystal disorder (degradation of diffraction, increase in mosaicity *etc.*). However, the exact mechanisms of both kinds of radiation damage and their relation to each other are not well understood. High-resolution X-ray diffraction experiments make it possible to investigate X-ray radiation-induced changes in the protein molecules in atomic detail, to visualize local structural changes and to provide insight into global changes.

The X-ray-induced local site-specific structural changes in protein molecules include the reduction of bound metal ions (Adam *et al.*, 2004; Yano *et al.*, 2005) and the breakage of some covalent bonds, with subsequent disordering of the atoms

involved in the disrupted bonds. Examples of X-ray-induced covalent-bond breakage are the disruption of disulfide bonds (Ravelli & McSweeney, 2000; Weik *et al.*, 2000; Burmeister, 2000); the rupture of covalent bonds between C and some heavy atoms, *e.g.* Se, Br, I and Hg (Evans *et al.*, 2003; Ramagopal *et al.*, 2005; Oliéric *et al.*, 2007); the decarboxylation of glutamate and aspartate residues (Ravelli & McSweeney, 2000; Burmeister, 2000; Fioravanti *et al.*, 2007; Petrova *et al.*, 2009) and the loss of the hydroxyl groups of tyrosines and the methylthio groups of methionines (Burmeister, 2000). It is believed that the atoms involved in ruptured bonds become mobile and diffuse through the sample. Nevertheless, sometimes they can be observed in the electron-density map in a new position close to their initial position (Ramagopal *et al.*, 2005). The occupancy values of these atoms in the crystallographic model decrease and their atomic displacement parameters (ADPs; also referred to as atomic *B* factors) increase. Interestingly, these local changes do not affect all residues equally. For example, some glutamate and aspartate residues rapidly become decarboxylated in proportion to the X-ray dose; however, some remain intact and appear to be highly resistant to damage (Petrova *et al.*, 2009).

The overall crystal radiation damage is manifested as a degradation of the crystal diffraction, changes in unit-cell parameters and an increase in the mosaicity and ADPs. It is generally accepted that these effects increase with the X-ray dose, which is defined as the energy absorbed per unit mass of a crystal (Sliz *et al.*, 2003; Shimizu *et al.*, 2007; Borek *et al.*, 2007).

The division of radiation damage into local and global damage is based on how the damage manifests itself as local or global effects. The radiation damage is also classified into two components depending on the physical phenomena that cause the damage. There are two components of radiation damage, the so-called primary damage, which results from the direct interaction of X-ray photons with the atoms of the sample, and the secondary damage, which is caused by the interaction of photoelectrons with protein and water, resulting in the generation of highly reactive radiolytic species which propagate through the crystal and cause further damage. The primary damage is largely independent of temperature (Teng & Moffat, 2002). The secondary damage is strongly dependent on temperature because it involves diffusion processes. At modern synchrotrons, X-ray diffraction data are usually collected at about 100 K, which greatly reduces the secondary radiation damage compared with the damage at room temperature (Nave & Garman, 2005; Southworth-Davies *et al.*, 2007). However, it is not entirely clear whether further lowering of temperature can significantly diminish secondary damage, although decreased damage at cryogenic temperatures below 100 K has been reported (Teng & Moffat, 2002; Meents *et al.*, 2010).

The majority of the specific local damage is believed to be a consequence of the secondary damage. The main arguments are firstly that the rate of local changes is much higher than that expected from direct interaction with X-ray photons (Holton, 2007) and secondly that the changes occur in an order that does not correspond to the probability of the absorption of photons by particular atoms and is more likely to be related to the strength of interatomic bonds (Garman & Owen, 2006). The global crystal damage is a result of collective damage effects; however, there is at present no consensus concerning the question whether, at a temperature of about 100 K, it is mainly caused by primary or secondary damage. Based on the experimentally observed linear dependence of radiation damage per incident photon on the coefficient of crystal absorption, Kmetko and coworkers concluded that the degradation of diffraction pattern at 100 K results mainly from primary damage (Kmetko *et al.*, 2006). In contrast, based on data on X-ray-induced changes in bond lengths in peptide crystals and radiolysis experiments, Meents and coworkers proposed that it is hydrogen abstraction from organic molecules with subsequent formation of gaseous hydrogen bubbles that causes global changes in the crystal (Meents *et al.*, 2009, 2010). Based on our recent experiments with aldose reductase, we suggested that the local damage is associated with global damage and that the linkage of these two processes is realised through the movement of protein domains and water molecules (Petrova *et al.*, 2009). Our experiments showed that irradiation induced the movement of large parts of the protein globule, which occurred simultaneously with the decarboxylation of Asp and Glu residues involved in intermolecular contacts and the rearrangement of the water network. This movement started at the initial stages of radiation damage and led to an increase in dynamic and static crystal disorder and correlates with expansion of the crystal unit cell. We believe that these are the main effects that contribute to the global damage to the protein crystal.

The present study of porcine pancreatic elastase confirms the X-ray-induced movement of protein domains. This protein was chosen because its crystals diffract to atomic resolution (∼1.10 Å), which allowed us to study damage at the atomic level, and because it contains four disulfide bridges, which are known to be prone to radiation damage (Helliwell, 1988; Berthet-Colominas *et al.*, 1999; Burmeister, 2000).

The X-ray-induced cleavage of disulfide bonds manifests itself as the gradual disappearance of electron density at the positions of the bonds in $2F_{\rm obs} - F_{\rm calc}$ maps. Numerous studies of different stages of crystal deterioration have been performed at relatively low resolution (Ravelli & McSweeney, 2000; Weik *et al.*, 2000, 2002; Burmeister, 2000; Banumathi *et al.*, 2004; Cianci *et al.*, 2008), which allowed the disappearance of electron density for the $S^{\gamma}-S^{\gamma}$ bond to be followed but did not allow modeling of how $S^{\gamma}-S^{\gamma}$ bond rupture proceeds at the atomic level. For example, several investigators have reported the appearance of positive electron density in $F_{\rm obs} - F_{\rm calc}$ difference maps in the close vicinity of deteriorated disulfide bonds. They suggested that this new density can be explained by either the appearance of new conformations of released cysteine residues (Burmeister, 2000; Banumathi *et al.*, 2004) or the divergence of two S^{γ} atoms (Cianci *et al.*, 2008), but did not model these new conformations because of the relatively low resolution. On the other hand, studies have been performed in which the deterioration of $S^{\gamma}-S^{\gamma}$ bonds

Table 1
Experimental settings and doses at each step of the experiment with crystal 1.

	No. of frames/exposure time for each frame (s)	Oscillation width (°)	Total exposure time (min)	Attenuation	Estimated flux (photons s^{-1})	Diffraction (Å)	Calculated dose per set (Gy)
Set 1	360/3	0.5	18	49.65	1.53×10^{10}	1.2	0.12×10^{7}
Set 2 'killing'	120/2	1.0	4	1		1.12	1.3×10^{7}
Set 3	360/3	0.5	18	49.65	1.49×10^{10}	1.5	0.12×10^{7}
Set 4 'killing'	120/2	1.0	4	1		1.4	1.3×10^{7}
Set 5	360/3	0.5	18	49.65	1.48×10^{10}	1.8	0.12×10^{7}
Set 6 'killing'	120/2	1.0	4	1		1.66	1.3×10^{7}
Set 7	360/3	0.5	18	49.65	1.45×10^{10}	2.0	0.12×10^{7}
Set 8 'killing'	120/2	1.0	4	1		1.82	1.3×10^{7}

has been investigated at very high resolution (Leiros *et al.*, 2001; Nukaga *et al.*, 2003) using only a single data set collected from each crystal, which did not allow the radiation-induced changes to be followed. In this study, we have filled this gap. We investigated the deterioration of disulfide bonds at different stages and at high resolution. Cysteine residues that participate in disulfide bonds were modeled as a mixture of initial and radiation-induced conformations at different stages of bond cleavage.

In order to monitor radiation damage at the level of single atoms, it was critical to begin and finish the diffraction experiment at high resolution. Multiple data sets corresponding to increasing doses were collected. This allowed us to record, at a decreased but still sufficiently high resolution, multiple snapshots of the progressive disruption of disulfide bridges and other changes in the structure. Domain movement was seen early in the experiment and occurred not only at 100 K but also at 15 K. Simultaneously, cleavage of disulfide bonds was observed, resulting in a loss of S^{γ} atoms, elongation of $S^{\gamma}-S^{\gamma}$ bonds and the gradual appearance of new cysteine rotamers, which occurred at both 100 and 15 K. Both kinds of radiation damage, local and global, evolve on approximately the same time scale and diminish similarly as the temperature decreases from 100 to 15 K. Thus, these experiments suggest that the correlation between local and global damage is revealed through X-ray-induced cooperative atomic movement.

2. Experimental procedures

2.1. Preparation of elastase crystals

Two crystals of elastase (referred to below as 1 and 2) were grown independently using different crystallization conditions. Crystal 1 was grown by the hanging-drop method at 297 K. The initial concentration of the protein was 10 mg ml^{-1} in water. The reservoir contained 25 m*M* Na_2SO_4 pH 8.2. The cryo-solution contained 25 m*M* Na_2SO_4 and 25% glycerol. The approximate dimensions of this crystal were $0.22 \times 0.10 \times 0.10$ mm. Crystal 2 was grown by the sitting-drop method at 291 K. The initial concentration of the protein was 20 mg ml^{-1} in 10% glycerol solution. The reservoir contained 250 m*M* Na_2SO_4 pH 7.5 (adjusted with NaOH). For cryo-protection, the 250 m*M* Na_2SO_4 was supplemented with 25% glycerol. The approximate dimensions of crystal 2 were $0.60 \times 0.15 \times 0.15$ mm. The content of solvent for both crystals was estimated to be 37%.

2.2. X-ray diffraction experiments

Two diffraction experiments were conducted independently on beamline 19-ID at the Advanced Photon Source (Argonne, USA; Rosenbaum *et al.*, 2006). The goal of the first experiment was to monitor the global and local changes that occur in the crystal as the delivered dose increases. During the experiment, eight data sets (sets 1–8) were consecutively collected from a single region of crystal 1 at 100 K. The crystal orientation, the rotation range, the energy of the X-ray beam (12.662 eV) and the crystal-to-detector distance (146 mm) were the same for all data sets. It was mentioned above that the approximate dimensions of this crystal were $0.22 \times 0.10 \times 0.10$ mm. In fact, this was an upper limit estimate (the actual dimensions were a little smaller). The crystal was oriented with the longest dimension along the spindle. The crystal and X-ray beam were visualized using the same microscope. The beam was imaged with phosphor. Slit sizes (0.05×0.1 mm; horizontal $\times$ vertical) were chosen so that the part of the crystal from which the data were collected was completely covered by the beam during the rotation of the crystal. Sets 1, 3, 5 and 7 were collected with an attenuated beam, while sets 2, 4, 6 and 8 ('killing') were collected without attenuation to enhance crystal damage. The photon flux density was calculated using records from the PIN diode, which was calibrated with the ion current of the ionization chamber. The flux of the slit X-ray beam was only measured for the attenuated beam. For the unattenuated beam, the flux was estimated using the attenuation coefficient (obtained from the calibration table). The dose absorbed by the crystal was calculated using the program *RADDOSE* (Murray *et al.*, 2004). The experimental settings and the calculated doses are summarized in Table 1. The total dose the crystal received by the end of the experiment was estimated to be 5.7×10^{7} Gy. This value exceeds the Henderson limit of 2×10^{7} Gy, which is theoretically determined as the dose the cryocooled crystal absorbs before the diffraction intensity decreases by half (Henderson, 1990), by a factor of $\sim$3 and exceeds the crystal radiation limit (3×10^{7} Gy), which is recommended based on experimental results as a maximum admissible dose for a protein crystal during data collection (Owen *et al.*, 2006), by a factor of $\sim$2. The deterioration of the crystal during the experiment manifested

Table 2
Experimental settings in the experiment with crystal 2.

	Data-collection temperature (A/B) (K)	Attenuation coefficient	No. of frames	Exposure (s)	Oscillation width (°)
Set 1a/set 1b	100/100	80.94	240	3	0.5
Set 2a/set 2b 'killing'	100/15	1.0	120	3	1.0
Set 3a/set 3b	100/100	80.94	240	3	0.5
Set 4a/set 4b 'killing'	100/15	1.0	120	3	1.0
Set 5a/set 5b	100/100	80.94	240	3	0.5

itself as a decrease in the maximum resolution limit from 1.2 to 1.82 Å; correspondingly, the number of measurements decreased by approximately fourfold (Table 3).

The goal of the second experiment, which was conducted with crystal 2, was to compare the character and the speed of X-ray-induced structural changes of the protein at two temperatures: 100 and 15 K. It has been reported that radiation damage varies considerably in different crystals of similar size (Nowak *et al.*, 2009). Our goal, therefore, was to perform the experiment at two temperatures at two different spots of the same crystal. We looked for a crystal that was homogeneous and long in one dimension. During this experiment, two series of data sets were collected from crystal 2: one series from region A and another series from region B. Each series consisted of five consecutive complete data sets (sets 1a–5a from region A and sets 1b–5b from region B). The experiment was performed on the same day. Firstly, sets 1b–5b were collected from part B; the crystal was set in the same orientation before each data collection. The crystal was then translated by 0.400 mm and sets 1a–5a were collected from part A. The irradiated areas of parts A and B were 0.350 mm apart. The experiment was designed so that the first, third and fifth data sets were collected at the same temperature, while the second and fourth sets (where the dose the crystal received was the greatest) were collected at different temperatures.

For both series, the first, third and fifth data sets (sets 1a, 3a, 5a and sets 1b, 3b and 5b) were collected at 100 K with the beam being attenuated about 81 times and the second and fourth sets (sets 2a and 4a and sets 2b and 4b) were collected using the unattenuated beam ('killing' sets). Sets 2a and 4a were collected at 100 K, while sets 2b and 4b were collected at 15 K. The dose the crystal received during each 'killing' set was 40 times higher than that received with the attenuated beam (Table 2). Thus, the greatest part of the dose was delivered during the collection of sets 2a and 4a in region A at 100 K and during the collection of sets 2b and 4b in region B at 15 K. The data collection at 15 K was conducted using a CRYOCOOL-LHe helium cryostat (CRYO Industries). The temperature of the cold gas stream was measured at the crystal position with a thermocouple calibrated with ice water and liquid nitrogen. The temperature of the gas stream was verified using an Si diode with standard curves. The energy of the beam was 12.665 eV and the crystal-to-detector distance was 110 mm. The crystal dimensions were 0.60 × 0.15 × 0.15 mm and the crystal was oriented so that its longest side was aligned along the spindle axis. The slit size of 0.05 × 0.2 mm (horizontal × vertical) was chosen so that the part of the crystal from which the data were collected was completely covered by the beam during crystal rotation. This was verified at both parts of the crystal. The dimensions of parts A and B were approximately equal. The fresh fraction of the crystal volume that entered and left the beam during rotation was zero. Therefore, the irradiated volumes of both part A and part B of the crystal during rotation in the beam were approximately equal. In this experiment, the dose value was not calculated. However, the conditions of the experiment and the values of the parameters that define the dose (the attenuation of the beam, the exposure time, the number of frames, the slit sizes and the irradiated volumes) were the same at both parts of the crystal. In addition, a comparison of I_0 recorded for each image during data collection for parts A and B suggests that the dose received by both regions of the crystal was approximately the same. Therefore, the doses that the crystal received during the experiment were approximately the same at both parts of the crystal. Details of the experimental procedure are given in Table 2.

2.3. Data processing and refinement of atomic models

All data sets were integrated and scaled using the *HKL-3000* structure-solution package (Minor *et al.*, 2006). The statistics for data processing and refinement are given in Tables 3 and 4. PDB entry 1gvk (0.95 Å resolution; Katona *et al.*, 2002) was used as a starting model for refinement. Models M1–M8, A1–A5 and B1–B5 were obtained in the course of refinement using data sets 1–8, 1a–5a and 1b–5b, respectively. Refinement was carried out using the *phenix.refine* package (Afonine *et al.*, 2005). Because the detector is heavily saturated during the collection of 'killing' data sets and many low-resolution reflections are missing, the low-resolution limit for refinement of the models corresponding to 'killing' sets was 10 Å. The refined parameters were the atomic coordinates, ADPs and the atomic occupancies for particular atoms and groups of atoms. For models M1, M2, M4, A1–A3 and B1–B3 the large number of observations allowed anisotropic refinement of the ADPs, while for models M3, M5–M8, A5 and B5 the refined ADPs were isotropic. In order to obtain accurate coordinates of atoms involved in disulfide bonds, the strength of geometrical restraints in the total refinement target was first decreased (the *wc* parameter was set to 0.5; by default, it is 1.0). Secondly, both Cys residues involved in each disulfide bridge were refined as independent conformers. For example, Cys136 and Cys201, which form a disulfide bridge, were modeled as *A* and *B* conformers, respectively. Examination of density maps and manual rebuilding of the model were performed using the program *Coot* (Emsley & Cowtan, 2004). During the first run for each refined model, only the coordinates and ADPs were refined. During all subsequent runs the occupancies were refined along with the atomic coordinates

Table 3
Data-processing and refinement statistics for the data sets collected from crystal 1.

Values in parentheses are for the last shell.

	Set 1	Set 2	Set 3	Set 4	Set 5	Set 6	Set 7	Set 8
Space group	$P2_12_12_1$							
Unit-cell parameters								
a (Å)	50.00	50.08	50.17	50.25	50.23	50.33	50.23	50.30
b (Å)	57.69	57.76	57.78	57.83	57.82	57.86	57.84	57.86
c (Å)	74.34	74.48	74.54	74.75	74.68	74.90	74.73	74.89
$\alpha = \beta = \gamma$ (°)	90	90	90	90	90	90	90	90
Resolution (Å)	1.2	1.12	1.5	1.4	1.8	1.66	2.0	1.82
No. of unique reflections	68040	80647	35266	43146	20478	26420	15168	20077
Completeness (%)	100 (99.9)	96.1 (82.4)	100 (100)	97.6 (99.3)	99.9 (100)	98.1 (98.9)	100 (100)	98.6 (99.4)
Multiplicity	7.0 (5.0)	4.2 (1.8)	7.1 (7.1)	4.7 (4.7)	7.0 (7.1)	4.7 (4.8)	7.0 (7.1)	4.7 (4.8)
$I/\sigma(I)$	33.7 (2.3)	20.6 (2.0)	33.4 (2.6)	25.9 (2.3)	26.5 (3.0)	25.2 (2.2)	22.5 (3.2)	23.4 (2.1)
$R_{\rm merge}$ (%)	3.9 (62.3)	7.2 (42.0)	3.6 (77.8)	5.7 (71.1)	4.7 (70.2)	5.3 (61.9)	5.3 (77.0)	5.1 (59.4)
Mosaicity (°)	0.45	0.55	0.54	0.64	0.65	0.71	0.73	0.76
$R_{\rm work}$ (%)	11.2	11.5	13.8	11.4	14.2	14.4	15.0	16.8
$R_{\rm free}$ calculated using 5% reflections (%)	13.9	14.1	16.9	15.8	19.9	21.5	22.9	23.5

Table 4
Data-processing and refinement statistics for data sets 1a, 2a, 3a and 5a collected from region A and data sets 1b, 2b, 3b and 5b collected from region B of crystal 2.

Values in parentheses are for the last shell.

	Set 1a	Set 1b	Set 2a	Set 2b	Set 3a	Set 3b	Set 5a	Set 5b
Space group	$P2_12_12_1$							
Unit-cell parameters								
a (Å)	50.02	50.00	50.03	49.99	50.16	50.11	50.24	50.12
b (Å)	57.76	57.79	57.74	57.78	57.83	57.79	57.87	57.76
c (Å	74.43	74.51	74.45	74.59	74.73	74.88	75.01	75.00
$\alpha = \beta = \gamma$ (°)	90	90	90	90	90	90	90	90
Resolution (Å)	1.1	1.1	1.1	1.1	1.4	1.4	1.75	1.55
No. of unique reflections	82585	85749	82126	80126	43068	42612	22232	31778
Completeness (%)	93.9 (84.5)	97.3 (90.3)	93.1 (92.5)	90.8 (92.1)	99.3 (99.7)	99.0 (98.6)	99.5 (99.7)	99.4 (99.0)
Multiplicity	3.5 (3.0)	4.3 (3.5)	3.6 (3.1)	4.0 (3.6)	4.4 (4.5)	4.4 (4.5)	4.4 (4.5)	4.4 (4.5)
$I/\sigma(I)$	26.2 (3.5)	26.5 (3.0)	22.8 (4.9)	19.6 (7.6)	34.7 (2.8)	29.2 (3.5)	30.5 (3.5)	28.7 (3.2)
$R_{\rm merge}$ (%)	2.5 (27.0)	3.1 (30.0)	4.1 (24.5)	5.6 (19.0)	2.1 (46.4)	2.4 (38.0)	2.7 (37.5)	2.6 (42.0)
Mosaicity (°)	0.28	0.31	0.38	0.42	0.46	0.42	0.56	0.50
$R_{\rm work}$ (%)	11.1	11.4	12.2	11.9	10.2	10.2	13.5	13.3
$R_{\rm free}$ calculated using 5% reflections (%)	13.3	13.1	14.7	13.8	14.7	14.2	20.0	17.6

and ADPs. Note that the occupancies were not refined for all atoms, but only for the atoms and groups of atoms for which negative electron density was observed in the $F_{\rm obs} - F_{\rm calc}$ map after the first refinement run. These were the atoms of Cys residues, the carboxyl groups of Glu70, Glu80, Asp164, Asp186 and Asp194 and a few water molecules. For a more detailed description of the modeling of disulfide bonds, see §3.2.1. Summaries of the refinement statistics and quality indicators of the models are presented in Tables 3 and 4.

2.4. PDB codes

Coordinates and structure factors have been deposited in the PDB with the following accession numbers: model M1, 100 K, 3mnb; model M2, 100 K, 3mnc; model M3, 100 K, 3mns; model M4, 100 K, 3mnx; model M5, 100 K, 3mo3; model M6, 100 K, 3mo6; model M7, 100 K, 3mo9; model M8, 100 K, 3moc; model A1, 100 K, 3mty; model A2, 100 K, 3odf; model A3, 100 K, 3mu0; model A5, 100 K, 3mu1; model B1, 15 K, 3mu4; model B2, 15 K, 3odd; model B3, 15 K, 3mu5; model B5, 15 K, 3mu8.

3. Results

The data sets analyzed in this study were collected using two crystals obtained in media with different salt concentrations; for crystal 1 (grown from 25 m*M* Na_2SO_4), eight data sets were collected with a total dose of 5.7×10^7 Gy, and for crystal 2 (grown from 250 m*M* Na_2SO_4), data sets were collected at two different temperatures. Qualitatively, X-ray-induced structural changes were similar in all experiments. Local structural changes and domain movements in refined models were analyzed as described previously (Petrova *et al.*, 2009).

3.1. X-ray-induced atomic movements

A comparison of the atomic coordinates for models corresponding to different stages of radiation damage revealed X-ray-induced displacements of the atoms of the elastase and water molecules. A similar phenomenon has recently been reported for aldose reductase (Petrova *et al.*, 2009). Similar to the aldose molecule, the molecule of elastase expands with the increase in the absorbed dose. The absolute values of atomic displacements averaged for all of the unit cells contributing to

Table 5
The numbers of protein atoms that moved over a distance greater than 0.1, 0.2, 0.3 and 0.4 Å relative to their positions in the undamaged model.

The number of well ordered protein atoms with full occupancy analyzed was 1587.

	Compared with model M1			Compared with model A1			Compared with model B1		
	M3	M5	M7	A2	A3	A5	B2	B3	B5
No. of protein atoms that moved over a distance greater than									
0.1 Å	753	1271	1334	123	861	1280	39	699	985
0.2 Å	153	546	661	6	117	533	2	40	194
0.3 Å	11	185	274	0	13	154	0	4	20
0.4 Å	0	54	112	0	1	28	0	1	7

diffraction are small; however, the movement is well defined. For example in data set M7 84% of well ordered protein atoms with full occupancy move more than 0.1 Å and 17% of atoms move more than 0.3 Å. The atoms begin to move as irradiation starts (Table 5). The shifts increase with the dose (Table 5) and correlate with changes in the unit-cell size.

The character of the structural changes of the protein molecule was analyzed using the difference distance matrix approach (Schneider, 2004) as implemented in the *RAPIDO* server (Mosca & Schneider, 2008; Mosca *et al.*, 2008). The method allows structurally invariant regions in the molecule, *e.g.* those parts of the structure that move approximately as rigid bodies, to be identified. Analysis of the data for elastase revealed two large fragments (shown in blue and green in Figs. 1*a* and 1*b*) that move as rigid bodies. Parts of the molecule that could not be assigned to structurally invariant regions were defined by the *RAPIDO* program as 'flexible' (shown in red in Figs. 1*a* and 1*b*). Thus, for elastase, as in the case of aldose reductase, irradiation causes the concerted movement of large protein domains. Note that the active site of elastase is in a region of contact between two domains (Fig. 1*c*). Two members of the catalytic triad, His57 and Asp102, belong to the first domain (blue), while the third member, Ser195, belongs to the second domain (green) (Fig. 1*c*). When the active site is composed of residues located in different protein domains, radiation-induced movement of these domains can be an additional factor affecting the catalytic site and enzyme activity. It has been observed previously that the residues of the active site are particularly sensitive to radiation damage and show a change in geometry and a large

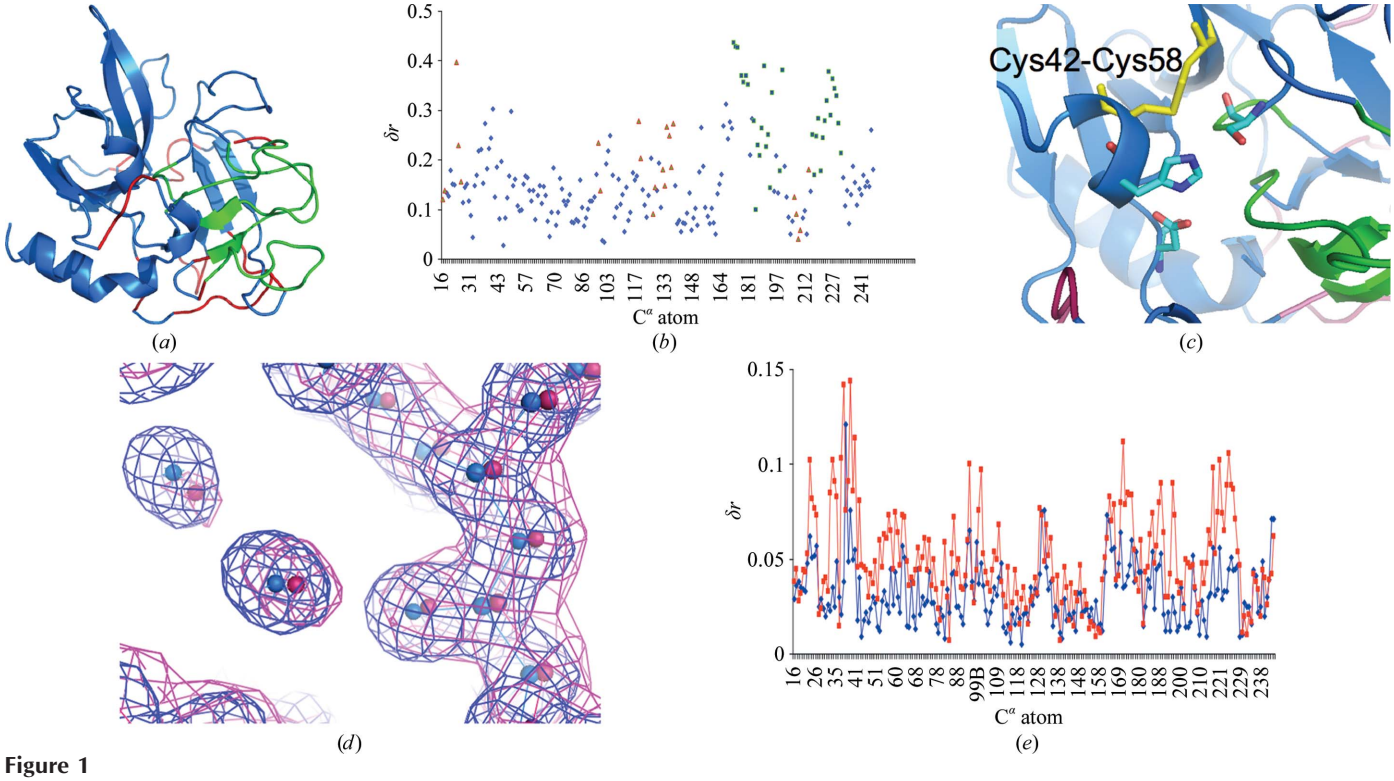

Figure 1
X-ray-induced displacements of elastase atoms and water molecules. (*a*) A schematic view of structurally invariant and flexible regions, as defined by the difference distance matrix implemented in the program *RAPIDO*. The atoms of the first and second structurally invariant regions are colored green and blue, respectively. Flexible regions are colored red. (*b*) The absolute values of atomic displacements of C^{α} atoms for model M5 relative to model M1. The difference in dose is 2.48×10^7 Gy. Only displacements of atoms in single conformations are shown. The colors correspond to those of the structurally conserved and flexible regions shown in (*a*). (*c*) An enlarged region of the active site of elastase. The residues of the catalytic triad, His57, Asp102 and Ser195 (shown in cyan), belong to different structurally conserved regions. The disulfide bridge Cys42–Cys58, which is damaged earlier than the other three bridges, is shown in yellow. (*d*) An enlarged region around H_2O 5, H_2O 6 and residues 163 and 164. The $2F_{obs} - F_{calc}$ electron-density maps for models M1 and M5 are contoured at 1.0σ and colored blue and pink, respectively. The atoms of models M1 and M5 are shown in blue and red, respectively. (*e*) Atomic displacements for model A2 relative to model A1 are shown in red. Atomic displacements for model B2 relative to model B1 are shown in blue. Only the displacements of well ordered C^{α} atoms with full occupancy are shown.

increase in ADP values (Weik *et al.*, 2000; Dubnovitsky *et al.*, 2005).

Water molecules in the vicinity of the protein surface move in concert with and in the same direction as the adjacent protein atoms (Fig. 1*d*).

The movement occurs at 100 K (data sets M and A) as well as (but to a lesser extent) at 15 K (data sets B). Model B2 was refined with data set 2b, which was collected at 15 K. The displacements of atoms in model B2 relative to the positions in model B1 (shown in blue in Fig. 1*e* for C^{α} atoms; see also Table 5) are very small. However, they clearly show that radiation-induced atomic movement occurs at 15 K. Thus, our experiments with elastase confirmed that radiation damage causes the cooperative movement of protein atoms and water molecules in crystals at 100 K and at temperatures as low as 15 K.

3.2. Breakage of disulfide bonds

3.2.1. Modeling of deteriorated disulfide bonds. The most prominent radiation-induced local structural damage to the elastase molecule is the breakage of disulfide bonds. All four disulfide bridges in the reference model are undamaged and 100% occupied. To model the radiation-induced changes with increased X-ray dose, the occupancy values of all cysteine residues were set to 1.0 and the atomic coordinates and ADP values were refined. The $F_{obs} - F_{calc}$ electron-density difference map was inspected. The negative density at S^{γ} atoms was an indicator of deterioration and was a motivation for further refinement of the occupancy values. An apparent positive density in the position of other rotamers of deteriorated residues was interpreted as the appearance of new conformations of cysteine residues (Figs. 2, 3 and 4). These conformations were modeled and refined. The occupancies of S^{γ} atoms were refined independently for each conformation of the same cysteine residue and independently for the cysteine residues of the same bridge. Thus, we obtained sequential models of disulfide-bridge deterioration as a function of increasing X-ray dose.

It has been shown by several investigators that different disulfide bridges of proteins exhibit variable susceptibility to radiation damage (Weik *et al.*, 2000; Leiros *et al.*, 2001). This is also true for elastase. The most susceptible to radiation damage is the Cys42–Cys58 bond, which is situated near the active site of the enzyme (Fig. 1*c*). The first slight sign of deterioration of this bridge is seen in model M1, which corresponds to an absorbed dose of 0.12×10^7 Gy (Table 1); all other bridges in M1 were unchanged. Similar dose values for the earliest signs of X-ray-induced damage to disulfide bonds have been reported elsewhere (Wang *et al.*, 2006; Shimizu *et al.*, 2007; Cianci *et al.*, 2008). In the experiment with crystal 2, all four disulfide bonds in models A1 and B1, which corresponded to the initial step of deterioration, were undamaged.

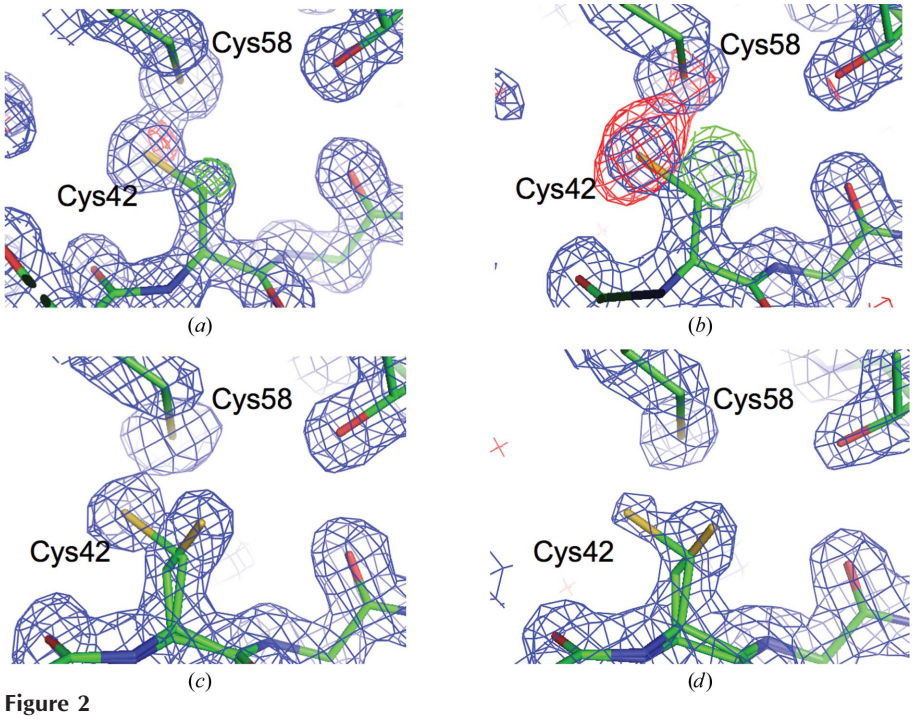

Figure 2
Radiation-induced changes of the bridge Cys42–Cys58. A decrease in the occupancy of S^{γ} atoms and the gradual appearance of a new rotamer of Cys42. (*a*) At the beginning of irradiation, the bridge is slightly damaged. The $2F_{obs} - F_{calc}$ density map for model M1 is shown in blue and contoured at 1σ. The positive and negative densities of the $F_{obs} - F_{calc}$ map for model M1 are contoured at $+2.25\sigma$ and -2.25σ and are colored green and red, respectively. (*b*) The appearance of negative density, which indicates a decrease in the occupancy values of the S^{γ} atoms of Cys42 and Cys58. The positive density indicates a new conformation of Cys42. The $2F_{obs} - F_{calc}$ electron-density map calculated for model M3, which contains only the initial conformations of Cys42 and Cys58 with full occupancy, is contoured at 1σ and colored blue. The positive and negative densities of the $F_{obs} - F_{calc}$ map for model M3 are contoured at $+3\sigma$ and -3σ and are colored green and red, respectively. (*c*) The $2F_{obs} - F_{calc}$ electron-density map calculated for model M3 with the initial and new conformations of Cys42. (*d*) The $2F_{obs} - F_{calc}$ electron-density map for model M5 with the initial and new conformations of Cys42.

3.2.2. Appearance of new rotamers of cysteine residues. As the delivered dose increased, we observed three types of effects on $S^{\gamma}-S^{\gamma}$ bonds: an increase in $S^{\gamma}-S^{\gamma}$ bond length (from 2.05 to 2.50 Å), a steady decrease in occupancy for all S^{γ} atoms and the appearance of new conformations for some cysteine residues. A second conformation of one of the cysteine residues is clearly seen in three disulfide bridges: Cys42–Cys58 (Fig. 2), Cys168–Cys182 (Fig. 3) and Cys191–Cys220 (Fig. 4). Note that one cysteine residue in each of these bridges has only a single conformation corresponding to the original position and the second cysteine residue assumes two conformations, both of which differ from the original position. At a dose of about 1.4×10^7 Gy, the occupancy of the second conformation of Cys42 exceeds the occupancy of the initial

conformation (Fig. 2*d*). When the dose is increased further, the occupancy values remain almost unchanged (Table 6). For the disulfide bridge Cys168–Cys182, the occupancies of the initial and new conformations become approximately equal, with the occupancy value of the initial conformation somewhat exceeding that of the new one (Fig. 3*d* and Table 6). For the disulfide bridge Cys191–Cys220 (Figs. 4*a* and 4*b*), the occupancy of the new conformation of Cys191 is small; the electron density corresponding to this conformation is not as strong as that corresponding to the new conformations for the residues of the disulfide bridges Cys42–Cys58 and Cys168–Cys182 and remains unchanged with increasing dose. Note that the sum of the occupancies of the initial and new conformations of the cysteine residue is less than 1.0 and is approximately equal to the occupancy of the second cysteine residue of the bridge (Table 6). This suggests that in addition to the breakage of the $S^{\gamma}-S^{\gamma}$ bond the breakage of some $C^{\beta}-S^{\gamma}$ bonds occurs or there are some additional minor cysteine conformations that we do not account for.

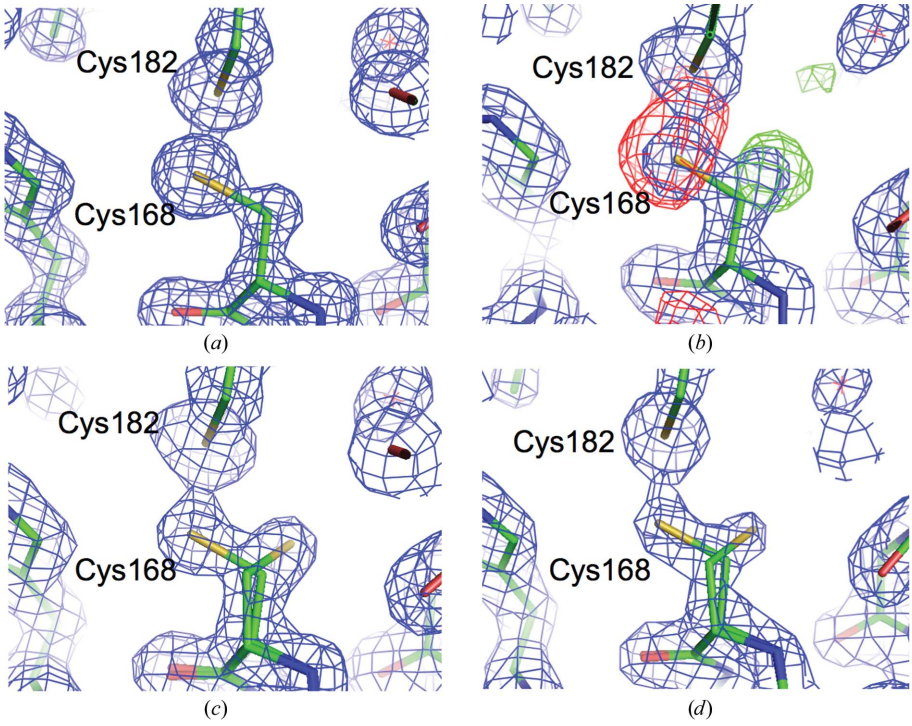

Figure 3
Radiation-induced changes of the bridge Cys168–Cys182. A decrease in the occupancy of S^{γ} atoms and the gradual appearance of a new rotamer of Cys168. (*a*) At the beginning of irradiation, the bridge is undamaged. The $2F_{obs} - F_{calc}$ density map for model M1 is shown in blue and contoured at 1σ. (*b*) The appearance of negative density, which indicates a decrease in the occupancy values of S^{γ} atoms of Cys168 and Cys182. The positive density indicates a new conformation of Cys168. The $2F_{obs} - F_{calc}$ electron-density map calculated for model M3, which contains only the initial conformations of Cys168 and Cys182 with full occupancy, is contoured at 1σ and colored blue. The positive and negative densities of the $F_{obs} - F_{calc}$ map for model M3 are contoured at $+3\sigma$ and -3σ and are colored green and red, respectively. (*c*) The $2F_{obs} - F_{calc}$ electron-density map calculated for model M3 with the initial and new conformations of Cys168. (*d*) The $2F_{obs} - F_{calc}$ electron-density map for model M5 with the initial and new conformations of Cys168.

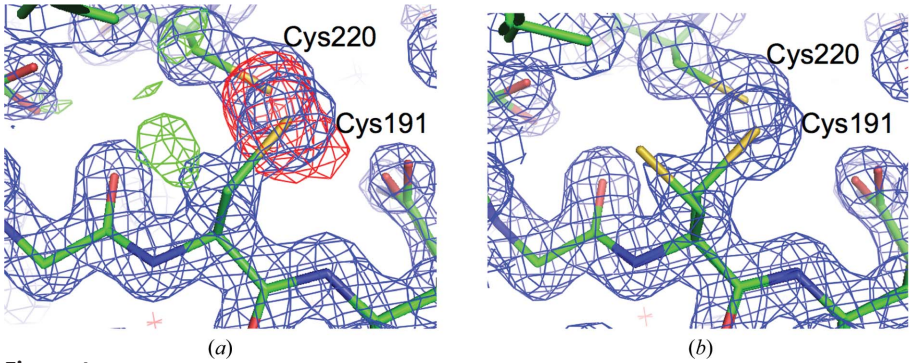

Figure 4
Radiation-induced deterioration of the bridge Cys191–Cys220. (*a*) The appearance of negative density, which indicates a decrease in the occupancy values of the S^{γ} atoms of Cys191 and Cys220. The positive density indicates a new conformation of Cys191. The $2F_{obs} - F_{calc}$ electron-density map calculated for model M3, which contains only the initial conformations of Cys191 and Cys220 with full occupancy, is contoured at 1σ and colored blue. The positive and negative densities of the $F_{obs} - F_{calc}$ map for model M3 are contoured at $+3\sigma$ and -3σ and are colored green and red, respectively. (*b*) The $2F_{obs} - F_{calc}$ electron-density map calculated for model M3 with initial and new conformations of Cys191.

A different behavior is observed for the fourth disulfide bridge Cys136–Cys201 (Fig. 5). The rate of decay of this disulfide bridge is similar to that of Cys191–Cys220, but there is no indication of a second conformation of the cysteine residues. The occupancy of the S^{γ} atoms of both Cys136 and Cys201 steadily decreases at an approximately equal rate. This suggests that in this case the rate of $C^{\beta}-S^{\gamma}$ bond breakage is very similar to that of $S^{\gamma}-S^{\gamma}$ bond breakage and no distinct new cysteine conformation is observed.

Our experiments revealed not only different susceptibilities of the $S^{\gamma}-S^{\gamma}$ bonds but also structural changes of different characters. It seems likely that two phenomena occur upon X-ray irradiation: a loss of S^{γ} atoms ($C^{\beta}-S^{\gamma}$ bond breakage), which is detected for all S^{γ} atoms, and the appearance of new cysteine rotamers, which is observed for some cysteine residues and disulfide bridges. An analysis of the decrease in occupancies suggests that the loss of S^{γ} atoms for each bridge occurs with approximately the same rate for both cysteine residues, suggesting a very similar rate for $C^{\beta}-S^{\gamma}$ bond breakage in the disulfide bridge. However, at a similar dose the rate is lower at lower temperature (see later).

3.2.3. Elongation of the S^{γ}—S^{γ} bond in disulfide bridges. As the dose increases, a slight but progressive elongation of the distance between S^{γ} atoms in the disulfide bonds is observed (Table 6). The value of this elongation is smaller than that reported by Weik *et al.* (2002). The maximal elongation is about 0.50 Å for the Cys42–Cys58 bond and about 0.20 Å for the other three disulfide bonds. The elongation occurs simultaneously with the displacement of the surrounding atoms of the main chain. This is clearly seen in the cases of Cys42–Cys58 and Cys136–Cys201 (Figs. 6 and 7).

It appears as if the radiation-induced movements of protein domains result in a slight divergence of parts of the main chain that are connected by disulfide bridges, which leads to a small elongation of the disulfide bonds. Presumably, this elongation is of a different origin than the elongation caused by electron capture of the bond and subsequent protonation (see §4).

Along with the electron density that corresponds to the new radiation-induced rotamers of cysteine residues, new positive electron-density peaks appear in close vicinity to almost all S^{γ} atoms in the difference $F_{obs} - F_{calc}$ map calculated for set 2 (Fig. 8). These peaks are found near all bridges at approximately equal distances from the S^{γ} atoms (about 0.9 Å). Similar peaks appear at the same positions in the difference maps calculated for set 2a and set 2b collected from crystal 2. The heights of these peaks vary, with the largest being twice the size of the electron density corresponding to well ordered H atoms. Similar peaks have been reported previously (Cianci *et al.*, 2008) and were interpreted as the new positions of the moving S^{γ} atoms of the splitting disulfide bond. In elastase these peaks appear at distances approximately equal to the distance between the C^{β} and S^{γ} atoms, which supports the hypothesis that these peaks correspond to new positions of S^{γ} atoms. However, in our experiments these peaks steadily decrease and finally disappear as the dose increases, underscoring their transitional character, in striking contrast to the electron densities corresponding to new cysteine rotamers. Note that these peaks also appear for the disulfide bridge Cys136–Cys201, which does not resolve into alternative conformations, unless the new conformation is very close to (overlaps with) the conformation that has an intact S^{γ}—S^{γ} bond. The disappearance of these peaks can be related to a decrease in resolution or to a particular transient intermediate state of the disulfide bond which is only observed at the initial stages of damage to the crystal (see §4).

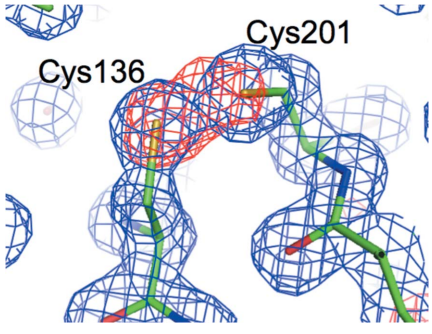

Figure 5
Radiation-induced deterioration of the bridge Cys136–Cys201. The appearance of negative electron density indicates a decrease in occupancy values for S^{γ} atoms. No new rotamers of cysteine residues appear. The $2F_{obs} - F_{calc}$ electron-density map for model M3 is contoured at 1.3σ and colored blue. The negative density of the $F_{obs} - F_{calc}$ map for model M4 is contoured at -2.8σ and is colored red.

3.3. Other specific radiation damage

The elastase contains four Glu and seven Asp residues. Only five of these residues are well ordered in the crystal structure. A decrease in the occupancy of the carboxyl group is observed for four of them (Glu80, Asp164, Asp186 and Asp194). Asp164 and Asp186, which are located on the surface of the protein, are damaged to a greater degree than the others. Glu80 is part of the metal-binding site and binds the sodium ion (the distance between Glu80 OE2 and the ion

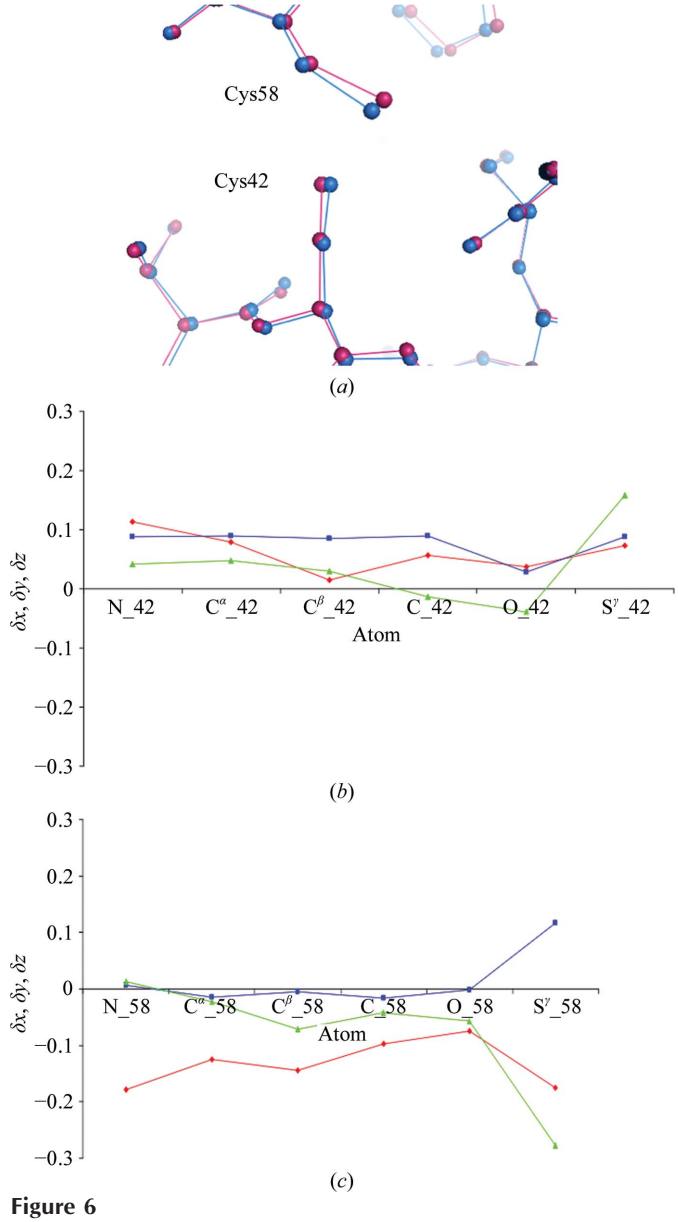

Figure 6
(*a*) Displacements of atoms in model M3 relative to their positions in model M1 in the region of the bridge Cys42–Cys58. (*b*, *c*) Displacements of atomic coordinates δx (shown in red), δy (shown in blue), δz (shown in green) for the atoms of Cys42 (*b*) and Cys58 (*c*).

Table 6
Changes in occupancy for S^{γ} atoms and $S^{\gamma}-S^{\gamma}$ distances for all disulfide bridges during the experiment with crystal 1.

The occupancy values divided by a slash correspond to the occupancies of S^{γ} atoms in the initial/new conformations of Cys residues. The $S^{\gamma}-S^{\gamma}$ distances are given between S^{γ} atoms of Cys residues in the initial/new conformation and other Cys residues of the bridge.

	Cys42–Cys58			Cys168–Cys182			Cys191–Cys220			Cys136–Cys201		
	S^{γ} occupancies		$S^{\gamma}-S^{\gamma}$ distance (Å)	S^{γ} occupancies		$S^{\gamma}-S^{\gamma}$ distance (Å)	S^{γ} occupancies		$S^{\gamma}-S^{\gamma}$ distance (Å)	S^{γ} occupancies		$S^{\gamma}-S^{\gamma}$ distance (Å)
Set 1	1.00	1.00	2.09	1.00	1.00	2.07	1.00	1.00	2.05	1.00	1.00	2.05
Set 2 'killing'	0.43/0.28	0.63	2.19/3.18	0.50/0.28	0.64	2.12/2.77	0.68	0.73	2.06	0.76	0.77	2.09
Set 3	0.34/0.36	0.63	2.40/3.23	0.41/0.34	0.66	2.12/2.77	0.60/0.13	0.71	2.12/3.69	0.73	0.75	2.17
Set 4 'killing'	0.27/0.35	0.54	2.42/3.28	0.37/0.35	0.62	2.19/2.98	0.50/0.10	0.55	2.13/3.52	0.67	0.69	2.20
Set 5	0.30/0.37	0.55	2.60/3.30	0.38/0.35	0.60	2.23/3.17	0.49/0.10	0.60	2.31/3.65	0.62	0.68	2.22
Set 6 'killing'	0.27/0.34	0.55	2.50/3.25	0.33/0.33	0.61	2.24/3.10	0.42/0.10	0.56	2.22/3.59	0.60	0.60	2.21
Set 7	0.27/0.34	0.55	2.76/3.27	0.32/0.33	0.61	2.38/3.35	0.42/0.10	0.56	2.36/3.24	0.60	0.60	2.30
Set 8 'killing'	0.27/0.37	0.49	2.65/3.32	0.32/0.33	0.61	2.25/3.16	0.41/0.10	0.56	2.25/3.39	0.61	0.65	2.26

Table 7
Changes in the occupancy of S^{γ} atoms and in $S^{\gamma}-S^{\gamma}$ bond lengths for the disulfide bridges in the experiment with crystal 2.

The values are given for models A1, A2, A3 and A5 and B1, B2, B3 and B5. The occupancy values divided by the slash correspond to the occupancies of S^{γ} atoms in the initial/new conformations of Cys residues. The $S^{\gamma}-S^{\gamma}$ distances are given between S^{γ} atoms of Cys residues in the initial/new conformation and other Cys residues of the bridge.

Model	A1	B1	A2	B2	A3	B3	A5	B5
Resolution (Å)	1.10	1.10	1.10	1.10	1.40	1.40	1.75	1.75
Bridge 42–58								
Occ. SG_42	1.0	1.0	0.50/0.21	0.73/0.08	0.39/0.36	0.58/0.18	0.26/0.35	0.49/0.32
Occ. SG_58	1.0	1.0	0.64	0.77	0.59	0.64	0.47	0.61
Length (Å)	2.05	2.06	2.17/3.13	2.10/2.92	2.29/3.15	2.13/3.04	2.43/3.22	2.17/3.05
Bridge 136–201								
Occ. SG_136	1.0	1.0	0.77	0.86	0.67	0.74	0.59	0.68
Occ. SG_201	1.0	1.0	0.75	0.86	0.74	0.77	0.63	0.71
Length (Å)	2.05	2.05	2.10	2.08	2.18	2.11	2.29	2.12
Bridge 168–182								
Occ. SG_168	1.0	1.0	0.56/0.22	0.68	0.47/0.32	0.63/0.13	0.32/0.28	0.52/0.23
Occ. SG_182	1.0	1.0	0.69	0.78	0.65	0.76	0.64	0.74
Length (Å)	2.05	2.06	2.11/2.66	2.07	2.19/2.86	2.07/2.68	2.15/2.99	2.05/2.70
Bridge 191–220								
Occ. SG_191	1.0	1.0	0.70/0.10	0.82	0.63/0.10	0.78	0.46/0.07	0.69/0.06
Occ. SG_220	1.0	1.0	0.70	0.82	0.64	0.79	0.62	0.78
Length (Å)	2.05	2.04	2.04/3.66	2.05	2.09/3.56	2.06	2.16/3.81	2.06/3.96

is 2.34 Å) and Asp194 participates in intermolecular contacts between strands. Interestingly, Asp102, which is part of the catalytic triad (His57, Asp102 and Ser195) in the active site and participates in four hydrogen bonds, is not damaged at all. No negative electron density in the difference $F_{\rm obs} - F_{\rm calc}$ density maps nor an increase in ADP values compared with those of the adjacent residues is observed for the Asp102 carboxyl group.

3.4. Comparison of X-ray-induced atomic displacements at 100 and 15 K

Data sets 1a and 1b were collected at the same temperature from different parts of the same crystal. Models A1 and B1, which were refined with these data sets, are virtually identical; the only exception is that their ADP values differ slightly. The mean values of the isotropic equivalents of ADPs for C^{α} atoms of residues in single conformations are 9.6 and 9.5 Å^2 for models A1 and B1, respectively. In both models, all disulfide bridges are undamaged and the isotropic equivalents of ADPs for the same S^{γ} atoms are virtually the same. ADPs are cumulative parameters which include the time- and space-averaged deviations of the atom position from its mean value (Trueblood *et al.*, 1996) and include experimental and computational errors. The equality of the isotropic equivalents of ADP values for the initial models A1 and B1 suggests that at the beginning of the experiment the contributions to ADP values from crystal disorder are very similar in both parts of the crystal.

Previously, we performed a similar experiment in which we collected data at different temperatures from two parts of the same crystal in order to reveal differences in atomic models at different temperatures (Petrova *et al.*, 2006). In this experiment, the data were collected with a highly attenuated beam to minimize radiation damage and to investigate the effect of temperature on the structure. The goal of the present study was to compare the radiation-induced structure deterioration at different temperatures. Models A2 and B2 were used for direct comparison of local damage at 100 and 15 K. Models A3 and B3 and models A5 and B5 are models of elastase at the same temperature; however, the fact that the greatest part of the dose was received by the crystal at different temperatures,

during 'killing' sets, makes these models well suited for comparison.

A comparison of the atomic coordinates of models A1, A2, A3 and A5 and models B1, B2, B3 and B5 shows that expansion of the protein molecule and displacement of water molecules are observed at both 100 and 15 K. The nature of the X-ray-induced expansion of the protein molecule is the same at both temperatures. However, the absolute values of the radiation-induced atomic displacements for models B2, B3 and B5 are smaller than those for models A2, A3 and A5, respectively (Table 5, Figs. 1*e* and 9*a*). Therefore, X-ray-induced collective domain movement still occurs at 15 K but its magnitude is smaller.

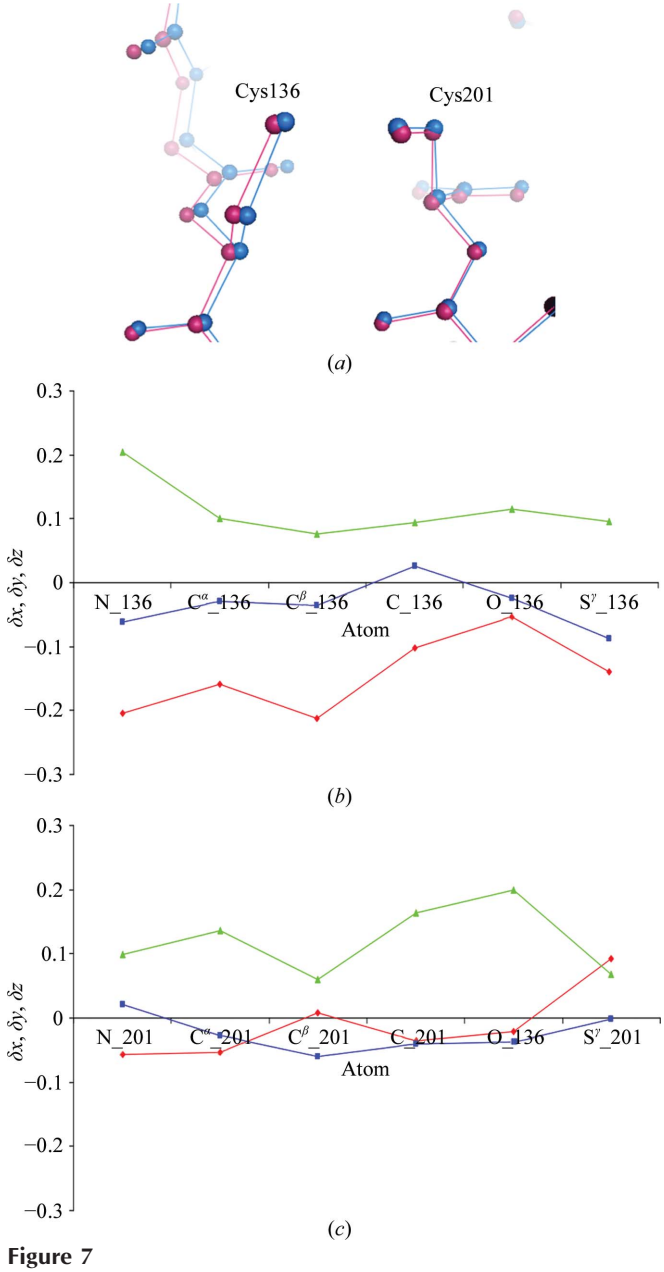

Figure 7
(*a*) Displacements of atoms in model M3 relative to their positions in model M1 in the region of the Cys136–Cys201 bridge. (*b*, *c*) Displacements of atomic coordinates δx (shown in red), δy (shown in blue), δz (shown in green) for the atoms of Cys136 (*b*) and Cys201 (*c*).

A comparison of the absolute values of atomic displacements for models B5 and A3 reveals approximately equal atomic shifts, the atomic shifts for model B5 being slightly greater than those for model A3 (Fig. 9*b* and Table 5). Because the dose the crystal received during the collection of each 'killing' set was 40 times higher than that received with the attenuated beam, the dose received during data collections with the attenuated beam can be neglected. Therefore, model B5 corresponds to an absorbed dose that is approximately twice the dose for model A3. However, a change in temperature from 15 to 100 K may introduce additional damage and therefore contribute to the total damage to models B3 and B5. Therefore, a factor of two is only a minimum limit. Thus, a dose more than two times larger must be delivered at 15 K to induce atomic displacements equal to those which occur at 100 K.

3.5. Comparison of X-ray-induced breakage of disulfide bonds at 100 and 15 K

The refined occupancies of all S^{γ} atoms that belong to cysteine residues in the initial conformation in models A2, A3 and A5 are smaller than those in models B2, B3 and B5, respectively (Table 7, Figs. 10 and 11). The occupancies of the new radiation-induced conformations of Cys42, Cys168 and Cys191 are higher in models A2, A3 and A5 than in models B2, B3 and B5 (Table 7, Fig. 12). Thus, both kinds of changes, the decrease in the occupancies of S^{γ} atoms and the appearance of new conformations, proceed more slowly at 15 K than at 100 K. The latter is pronounced when the Cys168–Cys182 bridge is compared in models A2 and B2. In the electron-density map for model A2 the new rotamer of Cys168 is clearly seen (Fig. 12*a*), while in the density map for model B2 it is absent (Fig. 12*b*).

A comparison of models B5 and A3 (Table 7) gives similar results. The occupancies of all S^{γ} atoms that belong to cysteine residues in the initial conformation in model A3 are smaller than the occupancies of these atoms in model B5; the occupancies of the new conformations in model A3 are higher than those in B5 (Figs. 10 and 12). Thus, the dose that induces similar deterioration of disulfide bonds at 15 K is approximately two times higher than at 100 K. However, taking into account that part B of the crystal was not kept at 15 K for the entire time, we suggest that a factor of two is only a minimum limit. The true value may be slightly higher.

4. Discussion

4.1. Reliability of occupancy values

The main indicator of structure deterioration in crystallography is a relative reduction of electron density in $2F_{\rm obs} - F_{\rm calc}$ maps and, as a consequence, an increase in the atomic ADP values and a decrease in occupancy for the corresponding atoms in the refined model. A decrease in occupancy is assumed to be equal to the fraction of protein copies with damaged residues in the volume of the crystal exposed to X-rays. The occupancy is obtained as a result of crystallo-

graphic refinement. Because the ADP values and the occupancy are intrinsically related to each other, diminishing of electron density can result from both an increase in ADP values and a decrease in occupancy for the corresponding group of atoms. During occupancy refinement for cysteine residues, we used the common approach in which the ADP values for atoms of cysteine residues are assumed to be approximately equal to the ADP values of the surrounding atoms (including the main chain), which supposedly have an occupancy equal to 1.0. For each run of refinement the starting isotropic equivalents of ADP values were the values obtained for the closest atoms of the main chain. After refinement, the approximate equality of the ADP values for all atoms of the bridge and the surrounding atoms was considered to be a criterion of the reliability of the refined occupancies and ADP values. A circumstance that also complicates the situation is that the steady crystal disordering that occurs in our experiments as the absorbed dose increases causes an increase in the atomic ADP values. These increases in ADP values are not equal for atoms of the main chain and the side chains. It is not known exactly how much the increase in ADP differs for the different atoms involved in the disulfide bridge and for the surrounding atoms. However, because we used the same procedure for all the bridges, we believe that the refined occupancies are reliable enough to compare the deterioration of different bridges and of the same bridges at different temperatures.

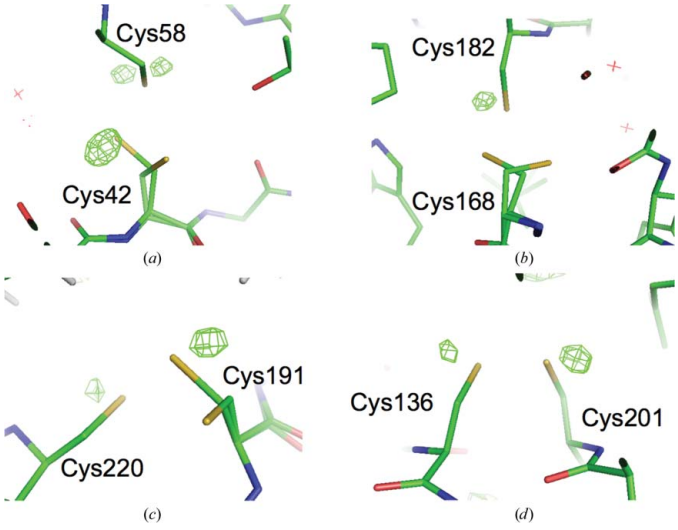

Figure 8
The appearance of new positive peaks in close vicinity to S^{γ} atoms in the difference $F_{obs} - F_{calc}$ map calculated for set 2. The $F_{obs} - F_{calc}$ electron density is shown in the vicinity of the bridges Cys42–Cys58 (*a*), Cys168–182 (*b*), Cys191–Cys220 (*c*) and Cys136–Cys201 (*d*) and is colored in green and contoured at +4.0σ (*a*), +5.5σ (*b*), +2.8σ (*c*) and +3.2σ (*d*).

4.2. The dependence of occupancy values of S^{γ} atoms on the delivered dose

The largest change in the occupancy of S^{γ} atoms of all cysteine residues is induced by the first portion of the dose at the beginning of irradiation. A similar dependence of the occupancy on the deposited dose has been observed previously, *e.g.* for X-ray-induced debromination in nucleic acids (Ennifar *et al.*, 2002; Schiltz *et al.*, 2004), and resembled first-order kinetics. A possible explanation of the behavior of the specific damage is the following: it seems likely that the specific protein damage mainly occurs as a result of secondary damage. It has been reported that the concentration of radiation-induced radicals in crystals at cryo-temperatures reaches saturation. At 77 K, half-saturation of X-ray-induced radicals was observed at 0.6 MGy, which is about 30 times less than the Henderson limit (Utschig *et al.*, 2008). Therefore, at the dose values normally used for data collection in macromolecular crystallography the concentration of radicals in the

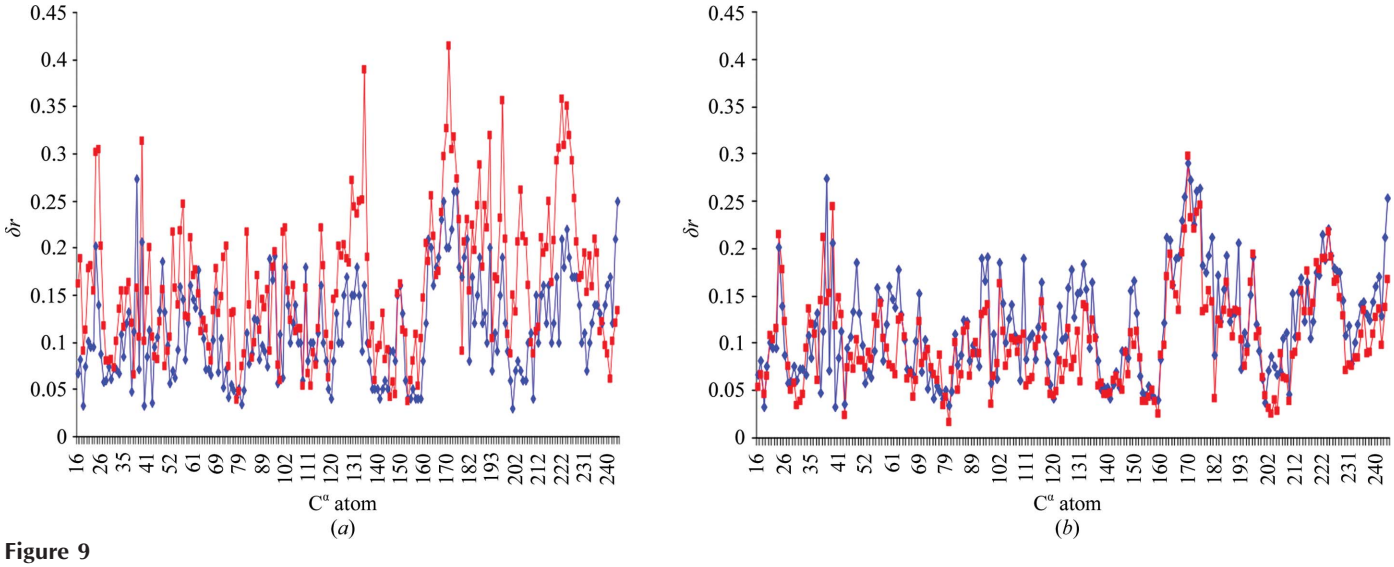

Figure 9
Comparison of the absolute values of radiation-induced atomic displacements δr at 15 and 100 K. (*a*) Atomic displacements for model A5 relative to model A1 are shown in red. Atomic displacements for model B5 relative to model B1 are shown in blue. (*b*) Atomic displacements for model A3 relative to model A1 are shown in red. Atomic displacements for model B5 relative to model B1 are shown in blue. Only the displacements of well ordered C^{α} atoms with full occupancy are shown.

sample is approximately constant, while the number of not yet damaged bonds susceptible to radiation decreases. As a result, the rate of the reaction decreases with an increase in dose. The occupancy values of the S atoms in the experiment with crystal 1 did not change after the crystal absorbed a dose of approximately 1.4×10^7 Gy, which is in agreement with this hypothesis.

4.3. Susceptibility of different bridges to radiation

It has been reported that residues of the same type within the same molecule exhibit different susceptibility to radiation (Ravelli & McSweeney, 2000; Fioravanti *et al.*, 2007; Holton, 2007). In the present study, the Cys42–Cys58 bridge is damaged at lower doses than the other three disulfide bridges and the Cys136–Cys201 bridge appears to be the most resistant to damage. However, the difference in the occupancies of the S^{γ} atoms of different bridges is only significant at the initial stages of damage. After a critical dose has been absorbed, the occupancy of S^{γ} atoms in different bridges does not change significantly. Interestingly, for almost all models the sums of the occupancies of the initial and new conformations of S^{γ} for Cys42, Cys168 and Cys191 do not differ significantly from the occupancy of Cys136, which is in a single conformation (Tables 6 and 7). For models M1–M8 the maximal difference is equal to 0.11 (for model M5 the sum of occupancies of the initial and new conformations of S^{γ} of Cys168 is equal to 0.73, while the occupancy of S^{γ} of Cys136 is equal to 0.62). For models A1–A5 and B1–B5 the maximal difference is equal to 0.14 (for model A3, the sum of occupancies of the initial and new conformations of S^{γ} of Cys168 is equal to 0.81, while the occupancy of S^{γ} of Cys136 is equal to 0.67). Thus, it seems likely that the main difference in radiation-induced changes for different disulfide bridges is the appearance of new conformers of cysteine residues.

For the residues of the Cys136–Cys201 bridge new cysteine rotamers do not appear. The atoms in the vicinity of this bridge are packed too close to Cys136 and Cys201, which may possibly make new conformers energetically unfavorable. For Cys136, two other alternate rotamers would be at a distance of approximately 2.4 Å from Leu199 or 1.7 Å from the O atom of Leu160. For Cys201, two other alternate rotamers would be at a distance of 2.1 Å from H_2O160 or 2.0 Å from His210 CD2. The bridge Cys136–Cys201 connects two antiparallel β-strands surrounded by other β-strands. It is likely that the packing of four β-strands is too rigid to allow new conformations of cysteine residues to arise.

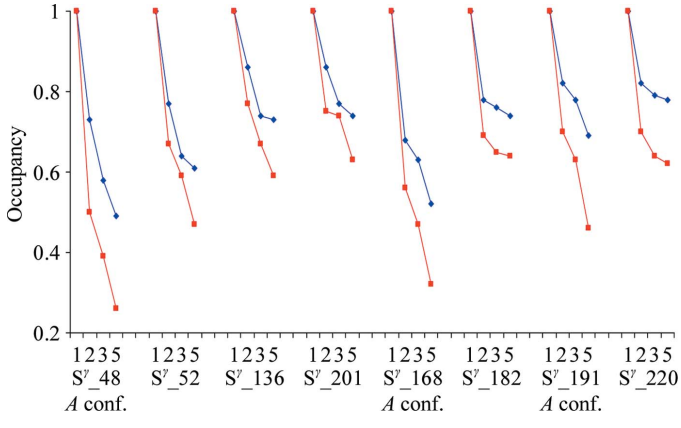

Figure 10
Occupancies of S^{γ} atoms for the initial conformations for all four bridges in models A1, A2, A3 and A5 (shown in red) and B1, B2, B3 and B5 (shown in blue). The occupancies of the S^{γ} atoms in model B5 are higher than those in model A3. This suggests that the dose that induces an approximately equal decrease in occupancies is at least two times higher at 15 K than at 100 K.

We calculated the water-accessible surface area using the program *AREAIMOL* from the *CCP*4 suite (Collaborative Computational Project, Number 4, 1994) for each S^{γ} atom (Table 8). A correlation between the water-accessible surface area and the occupancies of new X-ray-induced conformations of cysteine residues is clearly seen. Leiros and coworkers investigated the susceptibility to irradiation of disulfide bridges in salmon trypsin (PDB entry 1hj8) and bovine trypsin (PDB entry 1hj9) and concluded that Cys191–Cys220 is the most fragile bridge. Trypsin has a fold very similar to that of elastase. However, in the structure of elastase the Cys191–Cys220 bridge is much less exposed to water compared with the trypsin structures 1hj8 and 1hj9 (Fig. 13) and is less susceptible to radiation damage compared with the bridges Cys42–Cys58 and Cys168–Cys182. This supports the numerous observations of a correlation between the susceptibility of disulfide bridges to radiation and accessibility to water (Weik *et al.*, 2000; Burmeister, 2000; Meents *et al.*, 2010). Moreover, in our experiments with elastase we observed a correlation between the accessibility of the bridges to water and the appearance of new radiation-induced conformations of cysteine residues, which suggests that reactions that involve the products of water radiolysis play an important role in disulfide-bond rupture (see below).

4.4. Elongation of the S^{γ}—S^{γ} bond: implications for the mechanism of S^{γ}—S^{γ} bond breakage

Disulfide bonds can be broken in a variety of reactions (Prutz *et al.*, 1989; Burmeister, 2000). These reactions include, for example, electron capture with subsequent spontaneous cleavage (1 and 2), electron capture with further protonation (1 and 3), the formation of an $RSSR^{+}$ radical (4 and 5) with further reactions with hydroxyl ions (6) and reaction with a hydroxyl radical (7):

$$RSSR + e^{-} \rightarrow [RSSR]^{\bullet -} \quad (1)$$

$$[RSSR]^{\bullet -} \rightarrow RS^{-} + RS^{\bullet} \quad (2)$$

$$[RSSR]^{\bullet -} + H^{+} \rightarrow RSH + RS^{\bullet} \quad (3)$$

$$RSSR \rightarrow [RSSR]^{\bullet +} + e^{-} \quad (4)$$

$$RSSR + OH^{\bullet} \rightarrow [RSSR]^{\bullet +} + OH^{-} \quad (5)$$

$$[RSSR]^{\bullet +} + OH^{-} \rightarrow RSOH + RS^{\bullet} \quad (6)$$

$$RSSR + OH^{\bullet} \rightarrow RSOH + RS^{\bullet}. \quad (7)$$

The exact mechanism of X-ray-induced S^{γ}—S^{γ} bond breakage in protein crystals at cryogenic temperatures is unknown.

Experimental data about the diffusion of hydroxyl ions and hydroxyl radicals at cryogenic temperatures of about 100 K

Table 8
Water-accessible surface area for S^{γ} atoms of all disulfide bridges.

Disulfide bridges are ranked according to their susceptibility to radiation. The radius of the probe solvent molecule was 1.4 Å.

	Water-accessible surface area (Å^2)
S^{γ} of Cys42	0.90
S^{γ} of Cys58	3.20
S^{γ} (*A*) of Cys168	0
S^{γ} of Cys182	1.50
S^{γ} (*A*) of Cys191	0
S^{γ} of Cys220	1.20
S^{γ} of Cys136	0
S^{γ} of Cys201	0

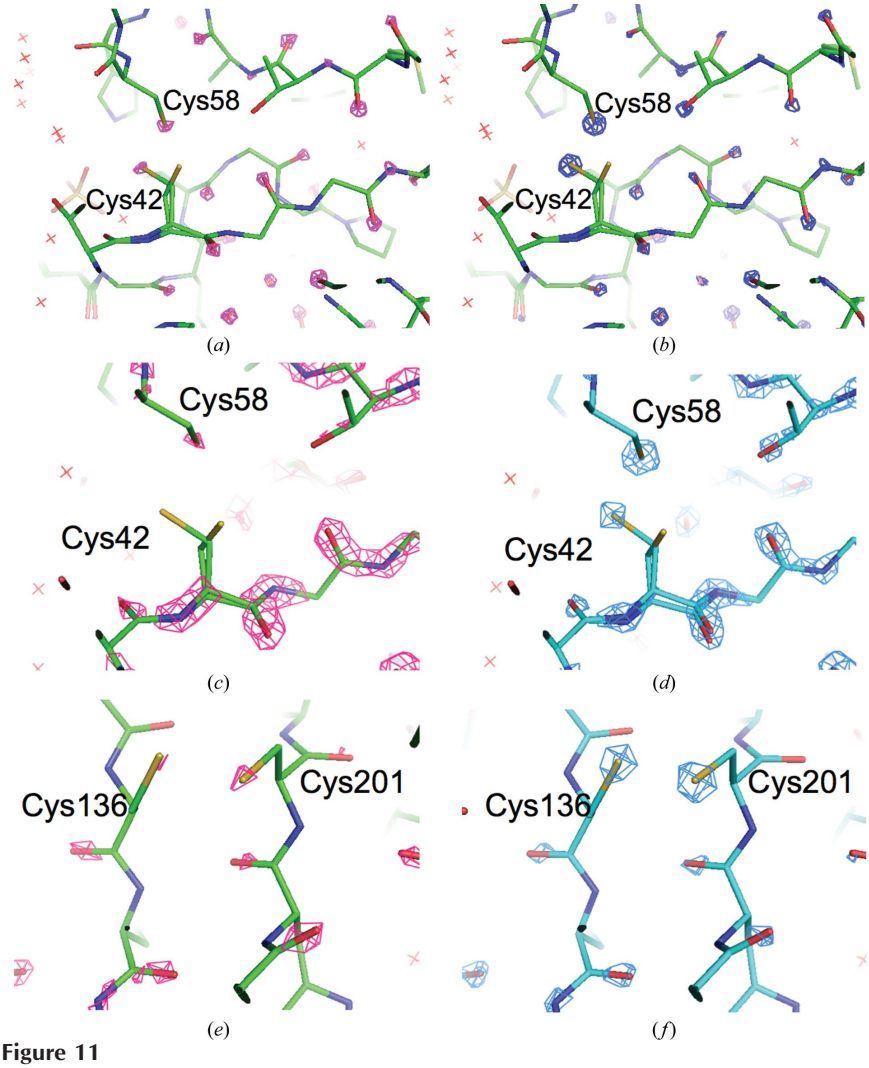

Figure 11
Comparison of the electron-density peaks for S^{γ} atoms for the cases in which the crystal was irradiated at 100 and 15 K. The levels of the $2F_{obs} - F_{calc}$ electron-density maps were chosen so that the maps had similar levels for the atoms of the main chain in the cases at 100 and 15 K. The electron density for S^{γ} atoms relative to the electron density for the main-chain atoms is higher at 15 K compared with 100 K. This indicates that the occupancies of S^{γ} atoms at 15 K are higher compared with those at 100 K. (*a*, *b*) $2F_{obs} - F_{calc}$ electron-density maps in the vicinity of the bridge Cys42–Cys58 for models A2 (*a*) and B2 (*b*) are shown in pink (for A2) and blue (for B2). Both maps are contoured at the same electron-density level of 2.19 e Å^{-3}. (*c*, *d*) $2F_{obs} - F_{calc}$ electron-density maps in the vicinity of the bridge Cys42–Cys58 for models A5 (*c*) and B5 (*d*) are shown in pink (for A5) and blue (for B5). (*e*, *f*) $2F_{obs} - F_{calc}$ electron-density maps in the vicinity of bridge Cys136–Cys201 for models A5 (*e*) and B5 (*f*) are shown in pink (for A5) and blue (for B5).

and below are scarce. It is believed that hydroxyl ions and hydroxyl radicals do not have high mobility at these temperatures and that the dominating mechanism is most likely through reactions with electrons (Kmetko *et al.*, 2006). It has been shown experimentally that at cryogenic temperatures electrons can migrate through the protein backbone owing to the tunneling effect (Symons, 1997). The disulfide bond is a strong electrophilic center and can capture a migrating electron. Several modeling studies have been performed with small disulfides (Berges *et al.*, 2000) and the protein thioredoxin (Rickard *et al.*, 2008) in which the geometry of S—S bonds in disulfide radicals in anionic and protonated forms were monitored. The initial coordinates were taken from crystallographic structures and were then optimized in a series of calculations using quantum-mechanical and molecular-mechanical (QM/MM) methods. These calculations showed that the addition of one electron to a single disulfide bridge weakens the bond and causes its elongation to 2.8 Å. A subsequent addition of a proton to this bond leads to an additional elongation to 3.5 Å. Weik and coworkers suggested that the measurement of the S^{γ}—S^{γ} bond in an irradiated crystal might provide insight into the mechanism of bond cleavage. Elongation of the S^{γ}—S^{γ} bond may be an indicator of either the creation of the anionic form of the disulfide radical or of its further protonation (Weik *et al.*, 2002). In a study with crystals that diffracted to 2.2 Å resolution initially and to 3.0 Å resolution at the end of the experiment, Weik and coworkers observed X-ray-induced elongation to 2.8 Å of one of the three disulfide bonds in the protein TcAChE and suggested that the corresponding cysteine was in an anionic form while the others were neutral.

In our experiments with elastase crystals, the elongation of the S^{γ}—S^{γ} bond was measured with a much higher accuracy. A steady radiation-induced elongation of the S^{γ}—S^{γ} bond was observed for all four disulfide bonds (§3.2.3). However, this increase did not exceed 0.5 Å, which is too small for the anionic form of the disulfide radical. Hence, the initial conformations of all bridges are likely to correspond to the neutral form of the disulfide bond.

As shown in §3.2.3, small peaks, which presumably correspond to S atoms with very low occupancies, arise in the difference electron-density map in the

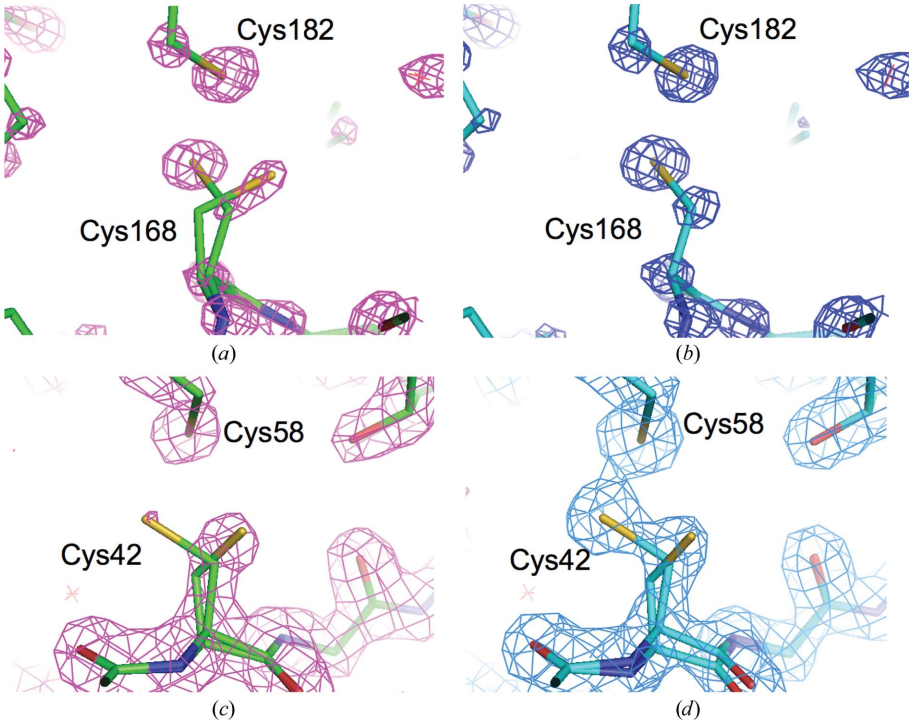

Figure 12
Appearance of new conformations of Cys residues for the cases where the crystal was irradiated at 15 and 100 K. (*a*, *b*) The $2F_{obs} - F_{calc}$ maps for models A2 (*a*) and B2 (*b*) are shown in pink (for A2) and blue (for B2). Both maps are shown in the vicinity of Cys168–Cys182 and are contoured at the same electron-density level of 0.69 e Å^{-3}. (*c*, *d*) The $2F_{obs} - F_{calc}$ maps for models A5 (*c*) and B5 (*d*) are shown in pink (for A5) and blue (for B5). Both maps are shown in the vicinity of Cys42–Cys58 and are contoured at the same level of electron density of 0.53 e Å^{-3}.

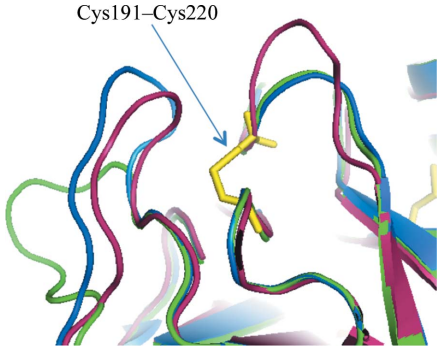

Figure 13
Comparison of elastase and two trypsin structures in the vicinity of the bridge Cys191–Cys220. In the structure of elastase, the bridge Cys191–220 is less exposed to the solvent than in the two trypsin structures. The structure of trypsin from Atlantic salmon (PDB entry 1hj8) is shown in green. The structure of bovine trypsin (PDB entry 1hj9) is shown in blue. The structure of elastase is shown in pink.

vicinity of almost all S^{γ} atoms at the initial stage of irradiation. There are two possible reasons why these peaks are only seen at the beginning of irradiation. Either they correspond to atoms with very low occupancy and are no longer seen as the resolution decreases, or they correspond to some temporary state of the disulfide bond which only arises at the initial stages of irradiation of the crystal. Because all these peaks are at almost equal distances from S^{γ} atoms of approximately 0.9 Å, one can speculate that these small peaks correspond to the elongated S—S bond in the disulfide radical of the anionic form. The rupture of the bond may occur either spontaneously (2) or as a result of further protonation (3). The proton may arise as a product of water radiolysis or through a hydrogen bond (sulfur can act as a hydrogen-bond acceptor). For elastase, the susceptibility of the bond to radiation damage correlates with the water-accessible surface area (Table 8), which may be an argument in favor of the hypothesis that it is the water-radiolysis products that participate in the reaction.

For all refined models, the distance between S^{γ} of the new rotamer of Cys42 and S^{γ} of Cys58 is in the range 3.18–3.32 Å (Tables 6 and 7) and the distance between S^{γ} of the new rotamer of Cys168 and S^{γ} of Cys182 is in the range 2.77–3.35 Å (Tables 6 and 7). Examination of the structures 1hj8 and 1hj9 of trypsin showed that the distances between the S^{γ} atom of the new conformation and the S^{γ} atom of the other cysteine involved in the bridge were 3.33 Å for the Cys22–Cys157 bridge, 3.25 Å for the Cys42–Cys58 bridge, 3.44 Å for the Cys168–Cys182 bridge and 3.21 Å for the Cys191–Cys220 bridge. All of these distances are less than the van der Waals radius of sulfur multiplied by two. In elastase crystals, the sum of the occupancies of the initial and new conformations of the cysteine residue is approximately equal to the occupancy of the second cysteine residue of the bridge. Both of these observations suggest that cysteine residues in new conformations interact with the second cysteine residue of the bridge and form disulfide radicals in the anionic or protonated form. However, this hypothesis calls for further modeling and experimental studies.

4.5. Temperature-dependence of disruption of disulfide bonds and atomic displacements

Because radiation damage presents a problem for structure determination (as well as structure interpretation) and sometimes even makes it impossible, investigation of ways to reduce crystal damage is very important. Compared with room temperature, at 100 K the crystal being irradiated retains its diffracting properties for a much longer time. Thus, it was found that the dose that can be delivered to a cryocooled macromolecular crystal before significant degradation of crystal order occurs is 70 times higher than the dose that can be given to a crystal at room temperature (Nave & Garman, 2005). Later, it was reported that cryocooling from room temperature to 100 K provides a 26–113-fold increase in the

lifetime of a crystal (Southworth-Davies *et al.*, 2007). Therefore, it is believed that cooling crystals to below 100 K may further decrease radiation damage to the protein crystal. Indeed, Teng and Moffat studied the decay of high-resolution reflections as a function of deposited dose at 40 and 100 K and showed that the quality of the diffraction data at 40 K was better than that at 100 K. However, the difference in quality was only obvious at deposited doses higher than 1.5×10^7 Gy (Teng & Moffat, 2002). It has also been shown that as the deposited dose increases the quality of the data collected from crystals cooled with a helium stream at 8 K is impaired more slowly than that of data collected from crystals cooled with nitrogen at 100 K (Chinte *et al.*, 2007). It was reported that the global radiation damage during data collection at 15 K was reduced by about 6% compared with that at 90 K for an insulin crystal and by about 23% in the case of crystals of holoferritin containing an iron core (Meents *et al.*, 2007). It was also demonstrated in experiments with D-xylose isomerase crystals that data collection at temperatures less than 20 K led to a 25% increase in the lifetime of high-resolution data compared with data collected from crystals cooled by a gaseous nitrogen stream at 100 K (Chinte *et al.*, 2007). Thus, reducing the temperature to below 100 K decreases global radiation damage to a macromolecular crystal. However, this decrease in damage is much less than the decrease in damage that occurs when going from room temperature to 100 K (Weik & Colletier, 2010).

A comparison of specific radiation damage to protein crystals at temperatures of 100 K and below has only been conducted in a few studies. Several reports have been devoted to decreasing damage to the active sites of metalloproteins (Yano *et al.*, 2005; Grabolle *et al.*, 2006; Corbett *et al.*, 2007) and one recent study was concerned with the deterioration of disulfide bonds at temperatures below 100 K (Meents *et al.*, 2010). It has been reported that X-ray-induced damage to the active site of metalloproteins at the liquid-helium temperature of 10 K decreases compared with X-ray-induced damage at 100 K (Yano *et al.*, 2005) and that the rate of photoreduction at 40 K is 40 times lower than that at 110 K (Corbett *et al.*, 2007). Very recently, Meents and coworkers reported that specific radiation damage to one disulfide bridge of cubic insulin which was exposed to solvent at 50 K was reduced by a factor of four compared with the damage at 100 K. Two other disulfide bridges, which were buried inside the molecule, exhibited only a very weak temperature-dependent susceptibility to radiation (Meents *et al.*, 2010).

Our experiments with elastase showed that decreasing the temperature from 100 to 15 K diminishes the deterioration of disulfide bonds and atomic displacement. The decrease in disulfide-bond deterioration was observed for all bridges and was estimated to be somewhat greater than twofold. The radiation-induced breakage of disulfide bonds and atomic displacement occurred on approximately the same time scale (slightly ahead of local damage), which was an indirect confirmation of the interrelation of these effects. As has previously been shown in our experiments with aldose reductase based on analyses of the anisotropy of ADPs (Petrova *et al.*, 2009), atomic displacements lead to an increase in the static disorder of the crystal because they occur at different speeds in different unit cells of the crystal. Thus, in the case of elastase, as with aldose reductase, both kinds of radiation-damage effects, local and global, evolve on approximately the same time scale. Because the damage at cryo-temperatures of about 100 K and below depends on dose, temperature and local solvent accessibility, it must be mostly caused by radiolytic species that are formed in the crystal solvent region. Changing the solvent properties to reduce the formation of radiolytic species or increase recombination events may lead to a reduction of radiation damage in macromolecular crystals.

The authors wish to thank the members of the Structural Biology Center at Argonne National Laboratory for their help with data collection on the 19-ID beamline. This work was supported by the US Department of Energy, Office of Biological and Environmental Research under contract DE-AC02-06CH11357, by the Centre National de la Recherche Scientifique (CNRS), by the Institut National de la Santé et de la Recherche Médicale and the Hôpital Universitaire de Strasbourg (H.U.S.) and by the Russian Foundation for Basic Research (grant 10-04-00254). The submitted manuscript has been created by UChicago Argonne, LLC, Operator of Argonne National Laboratory ('Argonne'). Argonne, a US Department of Energy Office of Science laboratory, is operated under Contract No. DE-AC02-06CH11357.

References

Adam, V., Royant, A., Nivière, V., Molina-Heredia, F. P. & Bourgeois, D. (2004). *Structure*, **12**, 1729–1740.
Afonine, P. V., Grosse-Kunstleve, R. W. & Adams, P. D. (2005). *CCP4 Newsl.* **42**, contribution 8.
Banumathi, S., Zwart, P. H., Ramagopal, U. A., Dauter, M. & Dauter, Z. (2004). *Acta Cryst.* D**60**, 1085–1093.
Berges, J., Fuster, F., Jacquot, J.-P., Silvi, B. & Houée-Levin, C. (2000). *Nukleonika*, **45**, 23–30.
Berthet-Colominas, C., Monaco, S., Novelli, A., Sibaï, G., Mallet, F. & Cusack, S. (1999). *EMBO J.* **18**, 1124–1136.
Borek, D., Ginell, S. L., Cymborowski, M., Minor, W. & Otwinowski, Z. (2007). *J. Synchrotron Rad.* **14**, 24–33.
Burmeister, W. P. (2000). *Acta Cryst.* D**56**, 328–341.
Chinte, U., Shah, B., Chen, Y.-S., Pinkerton, A. A., Schall, C. A. & Hanson, B. L. (2007). *Acta Cryst.* D**63**, 486–492.
Cianci, M., Helliwell, J. R. & Suzuki, A. (2008). *Acta Cryst.* D**64**, 1196–1209.
Collaborative Computational Project, Number 4 (1994). *Acta Cryst.* D**50**, 760–763.
Corbett, M. C., Latimer, M. J., Poulos, T. L., Sevrioukova, I. F., Hodgson, K. O. & Hedman, B. (2007). *Acta Cryst.* D**63**, 951–960.
Dubnovitsky, A. P., Ravelli, R. B. G., Popov, A. N. & Papageorgiou, A. C. (2005). *Protein Sci.* **14**, 1498–1507.
Emsley, P. & Cowtan, K. (2004). *Acta Cryst.* D**60**, 2126–2132.
Ennifar, E., Carpentier, P., Ferrer, J.-L., Walter, P. & Dumas, P. (2002). *Acta Cryst.* D**58**, 1262–1268.
Evans, G., Polentarutti, M., Djinovic Carugo, K. & Bricogne, G. (2003). *Acta Cryst.* D**59**, 1429–1434.
Fioravanti, E., Vellieux, F. M. D., Amara, P., Madern, D. & Weik, M. (2007). *J. Synchrotron Rad.* **14**, 84–91.
Garman, E. F. & Owen, R. L. (2006). *Acta Cryst.* D**62**, 32–47.

Grabolle, M., Haumann, M., Müller, C., Liebisch, P. & Dau, H. (2006). *J. Biol. Chem.* **281**, 4580–4588.
Helliwell, J. R. (1988). *J. Cryst. Growth*, **90**, 259–272.
Henderson, R. (1990). *Proc. R. Soc. Lond. B. Biol. Sci.* **241**, 6–8.
Holton, J. M. (2007). *J. Synchrotron Rad.* **14**, 51–72.
Katona, G., Wilmouth, R. C., Wright, P. A., Berglund, G. I., Hajdu, J., Neutze, R. & Schofield, C. J. (2002). *J. Biol. Chem.* **277**, 21962–21970.
Kmetko, J., Husseini, N. S., Naides, M., Kalinin, Y. & Thorne, R. E. (2006). *Acta Cryst.* D**62**, 1030–1038.
Leiros, H.-K. S., McSweeney, S. M. & Smalås, A. O. (2001). *Acta Cryst.* D**57**, 488–497.
Meents, A., Dittrich, B. & Gutmann, S. (2009). *J. Synchrotron Rad.* **16**, 183–190.
Meents, A., Gutmann, S., Wagner, A. & Schulze-Briese, C. (2010). *Proc. Natl Acad. Sci. USA*, **107**, 1094–1099.
Meents, A., Wagner, A., Schneider, R., Pradervand, C., Pohl, E. & Schulze-Briese, C. (2007). *Acta Cryst.* D**63**, 302–309.
Minor, W., Cymborowski, M., Otwinowski, Z. & Chruszcz, M. (2006). *Acta Cryst.* D**62**, 859–866.
Mosca, R., Branetti, B. & Schneider, T. R. (2008). *BMC Bioinformatics*, **9**, 352–368.
Mosca, R. & Schneider, T. R. (2008). *Nucleic Acids Res.* **36**, W42–W46.
Murray, J. W., Garman, E. F. & Ravelli, R. B. G. (2004). *J. Appl. Cryst.* **37**, 513–522.
Nave, C. & Garman, E. F. (2005). *J. Synchrotron Rad.* **12**, 257–260.
Nowak, E., Brzuszkiewicz, A., Dauter, M., Dauter, Z. & Rosenbaum, G. (2009). *Acta Cryst.* D**65**, 1004–1006.
Nukaga, M., Mayama, K., Hujer, A. M., Bonomo, R. & Knox, J. R. (2003). *J. Mol. Biol.* **328**, 289–301.
Oliéric, V., Ennifar, E., Meents, A., Fleurant, M., Besnard, C., Pattison, P., Schiltz, M., Schulze-Briese, C. & Dumas, P. (2007). *Acta Cryst.* D**63**, 759–768.
Owen, R. L., Rudiño-Piñera, E. & Garman, E. F. (2006). *Proc. Natl Acad. Sci. USA*, **103**, 4912–4917.
Petrova, T., Ginell, S., Mitschler, A., Hazemann, I., Schneider, T., Cousido, A., Lunin, V. Y., Joachimiak, A. & Podjarny, A. (2006). *Acta Cryst.* D**62**, 1535–1544.
Petrova, T., Lunin, V. Y., Ginell, S., Hazemann, I., Lazarski, K., Mitschler, A., Podjarny, A. & Joachimiak, A. (2009). *J. Mol. Biol.* **387**, 1092–1105.
Prutz, W. A., Butler, J., Land, E. J. & Swallow, A. J. (1989). *Int. J. Radiat. Biol.* **55**, 539–556.
Ramagopal, U. A., Dauter, Z., Thirumuruhan, R., Fedorov, E. & Almo, S. C. (2005). *Acta Cryst.* D**61**, 1289–1298.
Ravelli, R. B. & McSweeney, S. M. (2000). *Structure*, **8**, 315–328.
Rickard, G. A., Berds, J., Houée-Levin, C. & Rauk, A. (2008). *J. Phys. Chem. B*, **112**, 5774–5787.
Rosenbaum, G. *et al.* (2006). *J. Synchrotron Rad.* **13**, 30–45.
Schiltz, M., Dumas, P., Ennifar, E., Flensburg, C., Paciorek, W., Vonrhein, C. & Bricogne, G. (2004). *Acta Cryst.* D**60**, 1024–1031.
Schneider, T. R. (2004). *Acta Cryst.* D**60**, 2269–2275.
Shimizu, N., Hirata, K., Hasegawa, K., Ueno, G. & Yamamoto, M. (2007). *J. Synchrotron Rad.* **14**, 4–10.
Sliz, P., Harrison, S. C. & Rosenbaum, G. (2003). *Structure*, **11**, 13–19.
Southworth-Davies, R. J., Medina, M. A., Carmichael, I. & Garman, E. F. (2007). *Structure*, **15**, 1531–1541.
Symons, M. C. R. (1997). *Free Radic. Biol. Med.* **22**, 1271–1276.
Teng, T.-Y. & Moffat, K. (2002). *J. Synchrotron Rad.* **9**, 198–201.
Trueblood, K. N., Bürgi, H.-B., Burzlaff, H., Dunitz, J. D., Gramaccioli, C. M., Schulz, H. H., Shmueli, U. & Abrahams, S. C. (1996). *Acta Cryst.* A**52**, 770–781.
Utschig, L. M., Chemerisov, S. D., Tiede, D. M. & Poluektov, O. G. (2008). *Biochemistry*, **47**, 9251–9257.
Wang, J., Dauter, M. & Dauter, Z. (2006). *Acta Cryst.* D**62**, 1475–1483.
Weik, M., Bergès, J., Raves, M. L., Gros, P., McSweeney, S., Silman, I., Sussman, J. L., Houée-Levin, C. & Ravelli, R. B. G. (2002). *J. Synchrotron Rad.* **9**, 342–346.
Weik, M. & Colletier, J.-P. (2010). *Acta Cryst.* D**66**, 437–446.
Weik, M., Ravelli, R. B. G., Kryger, G., McSweeney, S., Raves, M. L., Harel, M., Gros, P., Silman, I., Kroon, J. & Sussman, J. L. (2000). *Proc. Natl Acad. Sci. USA*, **97**, 623–628.
Yano, J., Kern, J., Irrgang, K.-D., Latimer, M. J., Bergmann, U., Glatzel, P., Pushkar, Y., Biesiadka, J., Loll, B., Sauer, K., Messinger, J., Zouni, A. & Yachandra, V. K. (2005). *Proc. Natl Acad. Sci. USA*, **102**, 12047–12052.